

Annual Review of Nuclear and Particle Science

Deep-Sea and Lunar Radioisotopes from Nearby Astrophysical Explosions

Brian D. Fields^{1,2,3} and Anton Wallner^{4,5,6}

¹Department of Astronomy, University of Illinois, Urbana, Illinois, USA;
email: bdfields@illinois.edu

²Department of Physics, University of Illinois, Urbana, Illinois, USA

³Illinois Center for Advanced Studies of the Universe, University of Illinois, Urbana, Illinois, USA

⁴Helmholtz-Zentrum Dresden-Rossendorf, Institute of Ion Beam Physics and Materials Research, Dresden, Germany; email: a.wallner@hzdr.de

⁵Research School of Physics, Australian National University, Canberra, Australia

⁶Institute of Nuclear and Particle Physics, Technische Universität Dresden, Dresden, Germany

ANNUAL
REVIEWS **CONNECT**

www.annualreviews.org

- Download figures
- Navigate cited references
- Keyword search
- Explore related articles
- Share via email or social media

Annu. Rev. Nucl. Part. Sci. 2023. 73:365–95

The *Annual Review of Nuclear and Particle Science* is online at nucl.annualreviews.org

<https://doi.org/10.1146/annurev-nucl-011823-045541>

Copyright © 2023 by the author(s). This work is licensed under a Creative Commons Attribution 4.0 International License, which permits unrestricted use, distribution, and reproduction in any medium, provided the original author and source are credited. See credit lines of images or other third-party material in this article for license information.



Keywords

supernovae, nucleosynthesis, r-process, accelerator mass spectrometry

Abstract

Live (not decayed) radioisotopes on the Earth and Moon are messengers from recent nearby astrophysical explosions. Measurements of ⁶⁰Fe in deep-sea samples, Antarctic snow, and lunar regolith reveal two pulses about 3 Myr and 7 Myr ago. Detection of ²⁴⁴Pu in a deep-sea crust indicates a recent r-process event. We review the ultrasensitive accelerator mass spectrometry techniques that enable these findings. We then explore the implications for astrophysics, including supernova nucleosynthesis, particularly the r-process, as well as supernova dust production and the formation of the Local Bubble that envelops the Solar System. The implications go beyond nuclear physics and astrophysics to include studies of heliophysics, astrobiology, geology, and evolutionary biology.

Contents

1. INTRODUCTION	366
2. OVERVIEW OF NEAR-EARTH SUPERNOVAE AND KILONOVAE	368
2.1. Nearby Supernova Damage to the Biosphere	369
2.2. Nearby Supernova Signatures: Live Radioisotopes	369
3. RADIOISOTOPE PRODUCTION AND DELIVERY TO THE SOLAR SYSTEM	371
3.1. Radioisotope Synthesis in Supernovae and Kilonovae	371
3.2. Radionuclides After the Explosion: Incorporation of Interstellar Dust and Cosmic Rays	374
3.3. Transport Into the Solar System: Supernovae and Interstellar Medium Models	375
4. DETECTION METHOD: ACCELERATOR MASS SPECTROMETRY	376
4.1. Sample Preparation: Separation, Purification, and Element Enrichment	377
4.2. Ion Production, Ion Transport, and Single-Atom Counting	378
5. MEASURED RADIONUCLIDES IN DEEP-SEA AND LUNAR ARCHIVES ..	379
5.1. Archives and Terrestrial Deposition	380
5.2. ^{60}Fe Measurements: Supernova Detections	381
5.3. ^{244}Pu Measurements: r-Process Detection	384
5.4. The $^{244}\text{Pu}/^{60}\text{Fe}$ Ratio	384
5.5. Other Radioisotope Experiments	385
6. CONSEQUENCES OF NEARBY SUPERNOVAE AND KILONOVAE	386
6.1. Origin of ^{60}Fe and Distances to Supernovae	386
6.2. Implications for r-Process Nucleosynthesis	387
6.3. Implications for Supernova Dust Production, Evolution, and Survival	388
6.4. Implications for the Solar Neighborhood: The Local Bubble	388
6.5. Impact on the Heliosphere and Biosphere	389
7. PROSPECTS FOR FUTURE WORK	389
8. CONCLUSIONS AND OUTLOOK	391

1. INTRODUCTION

Astrophysics in the twenty-first century has opened new vistas to the cosmos by expanding the array of messengers available to bring us information about the Universe. These famously include signals from distant extragalactic relativistic sources: gravitational radiation originating in compact binary mergers (1, 2), as well as petaelectronvolt neutrinos arising from supermassive black holes—from both AGN jets (3, 4) and possibly tidal disruption of stars (5). In this review, we survey another new messenger, this one originating nearby: live (not decayed) radioactive isotopes found in natural terrestrial and lunar archives and arising from recent close-by astrophysical explosions.

Powerful explosions seem to be necessary to produce radioisotopes and deliver them to the Earth prior to decay; the most promising candidates are supernovae (SNe) and kilonovae. SNe play a central role in astrophysics, one of the most important being that they are element factories (6, 7) that drive Galactic chemical evolution. They produce many of the heavy elements (“metals”) in the cosmos and the bulk of the most common metals (8, 9). While most SN products are stable, the blizzard of nuclear reactions before and during the explosion also produce radioisotopes

spanning a wide range of lifetimes. Short-lived radioactivities have been directly observed in gamma-ray lines from ^{56}Ni decay in SN outbursts and via ^{44}Ti lines in the remnants of recent explosions (10). Longer-lived (lifetimes $\tau \gtrsim 1$ Myr) radioisotopes that are gamma emitters have also been detected, with ^{26}Al and ^{60}Fe sky surveys mapping recent Galactic nucleosynthesis (11).

Kilonova or macronova explosions result from mergers of two neutron stars or of a neutron star and black hole (12). The resulting coalescence is expected to produce a black hole, but some neutron star material can escape, ejected in tidal tails or in an accretion disk wind. As this neutron-rich material decompresses, it undergoes reactions far from nuclear stability, producing a vast array of radioisotopes up to and including actinides by the so-called r-process (13, 14). The decay of these species powers a kilonova outburst as seen in coincidence with gravitational radiation in the GW170817 event (15).

As we discuss in detail below, nearby explosions are an inevitable hazard of life in a star-forming galaxy such as ours. Most Galactic SNe and kilonovae safely occur many kiloparsecs away, and during written human history some have even been obscured from view, passing unnoticed (16–18). But over the ~ 4.5 Gyr age of the Earth, SNe likely occurred well within ~ 100 pc. Events at this uncomfortably close range threaten the biosphere and could even cause a mass extinction. Furthermore, nearby explosions deliver some of their debris to Earth. Stellar ejecta literally rain down slowly in minute amounts, accumulating a total of $\lesssim 1$ μg for every square centimeter on Earth. This offers the possibility of recovering this SN debris and using geological samples as telescopes to probe prehistoric explosions. But to discriminate this tiny dusting of extraterrestrial matter requires that we search for live radioactivity, which has little or no background. This comes at the price of an even smaller signal: femtograms per square centimeter.

Remarkably, suitable geological and lunar samples have been identified that serve as natural archives for prehistorical SN¹ and kilonova debris; one of these appears in **Figure 1**. Reading these isotopic fossils requires the powerful method of accelerator mass spectrometry (AMS), which permits the detection of individual trace radioactive atoms. As detailed below, AMS measurements now reach levels of $^{60}\text{Fe}/\text{Fe} \lesssim 10^{-17}$ and, thereby, have found a wealth of data. A pulse of ^{60}Fe appears in deep ocean samples around the world (20–24). The signal arrival is around

$$t(\text{SN Plio}) \simeq 3.5 \text{ Myr ago}, \quad 1.$$

and its likely origin has been dubbed the Pliocene supernova (SN Plio) (25) to reflect the corresponding geological epoch. A second, earlier pulse has been found (23, 24), arriving around

$$t(\text{SN Mio}) \simeq 8 \text{ Myr ago}, \quad 2.$$

and its likely origin has been called the Miocene supernova (SN Mio). ^{60}Fe is also seen in modern Antarctic snow (26), in Apollo lunar samples (27), and in cosmic rays (28).

All of these measurements together give compelling evidence that there were multiple near-Earth explosions—likely SNe—in the past 10 Myr, that their effects linger to the present day, and that they played a role in sculpting the Local Bubble in which the Solar System resides. These discoveries have also driven a search for other radioisotopes, leading to the detection of ^{244}Pu in samples that are not well dated but overlap both ^{60}Fe pulses (24). This discovery has profound implications because ^{244}Pu is one of the heaviest known nuclei and is only made in the so-called r-process, the cosmic origin of which remains one of the most pressing questions in astrophysics

Parsec (pc):

1 pc = 3×10^{18} cm,
which is roughly the
typical separation
between neighboring
stars in our Galaxy

¹“Historical SNe” are those with surviving eyewitness accounts; such records reach back about 2,000 years (19). Here we are interested in “prehistorical SNe” going back many millions of years, where the evidence is isotopic and whose observers left no surviving records.



Figure 1

A ferromanganese (FeMn) crust from the Pacific Ocean, 237KD. AMS measurements of this crust have found interstellar ^{60}Fe (21, 22, 35), ^{53}Mn (36), and ^{244}Pu (35, 37). It covers more than 20 Myr of nuclide incorporation. The coin for scale has a diameter of 3.2 cm. Abbreviation: AMS, accelerator mass spectrometry. Photograph provided by D. Koll.

today. The observed ^{244}Pu may point to a SN or kilonova origin; future ^{244}Pu measurements could address the site of the r-process.

In this article, we review the emerging study of near-Earth explosions that deposit ejecta on the Earth and Solar System, focusing on SNe and kilonovae. The subject is inherently interdisciplinary, and we hope this discussion is accessible to a broad audience, particularly for nuclear and particle physicists as well as astrophysicists. Other recent overviews have focused on astrophysics (29), nucleosynthesis (30), heliophysics (31), and mass extinctions (32). More details on experimental aspects of ^{60}Fe and ^{244}Pu measurements and their interpretations are found in References 33 and 34.

We summarize in Section 2 how this subject arose and evolved in the literature. We then trace the journey of radioisotopes in Section 3, from their nucleosynthesis to their sequestration into dust grains, to their transport from the explosion to the Solar System. In Section 4, we explain the AMS technique that allows for ultrasensitive radioisotope measurements, whose results we discuss in Section 5. We discuss in Section 6 the consequences that span many areas of astrophysics and beyond to nuclear physics, heliophysics, astrobiology, geology, and possibly planetary science and evolutionary biology. In Section 7, we suggest possible future directions for the field, and we summarize our conclusions and outlook in Section 8.

2. OVERVIEW OF NEAR-EARTH SUPERNOVAE AND KILONOVAE

As the observational and theoretical picture of SNe has come into focus, the question quickly arose: How would a nearby explosion affect the Earth, and what signatures would nearby events leave? Early work focused on SN production of ionizing radiation and the possible biological damage that could result. As early as 1950, the paleontologist Otto Schindewolf suggested that SNe could play a role in biological mass extinction via their production of cosmic rays (38, 39). Around the same time, Iosif Shklovsky and his group pioneered the astrophysics of this idea (40, 41): They calculated rates of nearby explosions, estimated the resulting cosmic-ray enhancement, proposed a SN origin for specific mass extinctions, and suggested that nearby SNe created large features in the radio and high-energy sky, now known as the North Polar Spur and Loop I.

2.1. Nearby Supernova Damage to the Biosphere

The mechanisms for nearby SN damage to the biosphere stem from the effects of ionizing radiation: high-energy γ rays, X-rays, and cosmic rays. These damaging particles are produced in different phases of the SN and its aftermath and, so, lead to a sequence of distinct threats to biota.

1. About 100 days after the explosion, the remnant becomes transparent to gamma rays, largely from $^{56}\text{Ni} \rightarrow ^{56}\text{Co} \rightarrow ^{56}\text{Fe}$ decay, and the resulting gamma-ray flux is sustained for about the first year.
2. After months to years, X-rays can arise from collisions between the blast and immediately surrounding material that had been ejected in a pre-SN wind; in a small but powerful subset of SNe (Type II_n), these can be bright for up to ~ 10 years.
3. Finally, after many thousands of years, cosmic rays arrive along with the blast itself that accelerates them; these remain intense for thousands of years.

Earth's atmosphere absorbs gamma rays, X-rays, and the lowest-energy cosmic rays, thereby shielding biota from direct injury by these particles. But Ruderman (42) pointed out that the consequence of this absorption is severe depletion of the stratospheric ozone, and the removal of this “umbrella” exposes the biosphere to a dramatic increase of harmful solar ultraviolet (UV) radiation. This effect is thus common to all of the SN damage phases listed above. Subsequent work explored ozone loss further, and atmospheric models of increasing sophistication were used to develop detailed predictions (43–45). The Kansas group has characterized how the ozone depletion varies over time and its dependence on the SN location in the sky, the photon energy spectrum, time of year, and other factors (46, 47). They identified the key factor to be the fluence (time integrated energy flux) of ionizing photons, which break apart N_2 and O_2 molecules. This creates nitrate ions, largely NO and NO_2 , that catalyze ozone destruction. A lethal dose of ionizing radiation that destroys $\sim 30\%$ of stratospheric ozone arises from a “kill fluence” of $\mathcal{F}_{\text{ionizing}} = 100 \text{ kJ m}^{-2}$; this leads to a SN “kill distance” of $\sim 8\text{--}10 \text{ pc}$ (42, 45, 46, 48, 49).

The biological consequences of a large ozone loss and UV increase are subjects of active research and likely to be complex (46). For example, this would lead to destruction of phytoplankton that represent a large fraction of Earth's photosynthesis. These organisms also lie at the base of the food chain, so their destruction would propagate upward to more complex organisms, potentially leading to a mass extinction.

While ozone loss is common to all three nearby-SN damage phases, cosmic rays pose additional threats arising from their interactions in the atmosphere (50, 51). Bombarding particles with energies $\gtrsim 1 \text{ GeV}$ interact with nucleons in the atmosphere to produce charged pions and in turn energetic muons, e.g., $p_{\text{cr}} + N_{\text{atm}} \rightarrow \pi^{\pm} \rightarrow \mu^{\pm}$. The muons penetrate matter and deliver harmful doses of ionizing radiation on the Earth's surface and hundreds of meters below. These likely have particularly damaging effects for large creatures (megafauna) on land and in the sea (52). Other effects of cosmic rays have been proposed, including increased lightning strikes and thus global fires (53) and effects on climate (54, 55).

2.2. Nearby Supernova Signatures: Live Radioisotopes

Starting in the 1960s it was noted that live radioisotopes could be a SN signature (58). A search of Apollo 11 lunar samples for ^{247}Cm and ^{244}Pu —assumed to be SN products—was used to claim limits on nearby SNe “within the last eon or two” (59, p. 500). Alvarez et al. (57) also identified ^{244}Pu as a close-by SN signature that would have little to no background. While their search excluded a SN origin of the Cretaceous-Tertiary [K-T, or Cretaceous Paleogene (K-Pg)] mass

NEARBY SUPERNOVAE AND THE DINOSAURS

Nearby SNe were proposed as the source of the K-Pg mass extinction that saw the demise of the dinosaurs (56). This possibility was considered in detail in the celebrated Alvarez et al. work (57), as an alternative to the impactor scenario they ultimately favored. These authors recognized that the SNe would deposit live radioisotopes on the Earth. They searched for and failed to find ^{244}Pu in material from the K-Pg boundary and used this nondetection to rule out a SN culprit. It is ironic that now the evidence is that most SNe do not make the r-process and, hence, do not produce ^{244}Pu (see Section 3.1), so its absence need not exclude a SN; but, of course, the discovery of the Chixulub crater verifies the Alvarez impactor hypothesis.

extinction (see the sidebar titled Nearby Supernovae and the Dinosaurs), live radioisotopes have proven to be powerful probes of nearby explosions.

Ellis et al. (60) considered the general problem of isotopic signatures from a near-Earth SN. They identified the importance of live radioisotopes, surveyed intermediate-lived species and their origins, and estimated signals as a function of SN distance, including for ^{60}Fe and ^{244}Pu . Independently, the Garching group proposed SN ^{60}Fe as a promising target for AMS (61) (see Section 4).

A few rough calculations highlight the likelihood of nearby explosions and the challenge of detecting them. We can estimate the rate of nearby SNe as follows. The Milky Way core-collapse (massive star) SN rate is $\dot{N}_{\text{SN}} \simeq 3$ events/century. The Milky Way thin disk is the site of star formation and, thus, SN explosions, and we model it with an exponential scale radius of $R_{\text{thin}} = 2.9$ kpc and a scale height $h_{\text{thin}} = 95$ pc (18, 62). This leads to a SN rate density $\mathcal{R}_{\text{SN}} = \dot{N}_{\text{SN}} e^{-R_{\odot}/R_{\text{thin}}} / 4\pi R_{\text{thin}}^2 h_{\text{thin}}$ at our location $R_{\odot} = 8.5$ kpc. Thus, in a sphere of radius $r < h_{\text{thin}}$, the rate of SNe is

$$\Gamma_{\text{SN}}(D_{\text{SN}}) \approx \frac{4\pi}{3} D_{\text{SN}}^3 \mathcal{R}_{\text{SN}} = (1.5 \text{ Myr})^{-1} \left(\frac{D_{\text{SN}}}{100 \text{ pc}} \right)^3 \left(\frac{\dot{N}_{\text{SN}}}{3 \text{ century}^{-1}} \right), \quad 3.$$

and we see that on average, SNe within 100 pc occur on ~ 1 -Myr timescales, and events as close as 10 pc can occur within the 4.5-Gyr lifetime of the Earth. Nearby SNe are thus common on astronomical and geological timescales, which is an inevitable consequence of life in our star-forming galaxy. For kilonovae, the rates are more uncertain but ~ 100 times smaller, so events over the same timescales occur at greater distances.

What traces will a nearby SN leave on Earth? A rough calculation idealizes the SN blast as a dense spherical shell that distributes material isotropically (60). This means that the integrated flux² (i.e., interstellar fluence) of SN ejecta at a distance D_{SN} from the explosion falls as the inverse square of the distance. Using this, we can estimate the bulk deposition of all SN heavy elements (“metals”) delivered to observers, neglecting the gaseous hydrogen and helium that will not leave direct geological signatures. Adopting an ejected metal mass $M_{\text{ej}} \sim 2 M_{\odot}$, i.e., twice that of the Sun, and a SN distance $D_{\text{SN}} = 10$ pc, we find the interstellar fluence impinging on the Solar System is $\mathcal{F}_{\text{SN}} = M_{\text{ej}} / 4\pi D_{\text{SN}}^2 \sim 0.3 \mu\text{g cm}^{-2}$. We see that even at this uncomfortably close distance, the deposition of bulk SN material is small: Each square centimeter of a Solar System body would at most collect on the order of a few micrograms of ejecta. This will not leave a visible layer as

²Key radioisotope observables are *interstellar flux* at the Sun’s location prior to any Solar System screening, the time-integrated flux (*fluence*), and the average *surface density on Earth*, which includes heliospheric screening effects and a factor of 1/4 for the ratio of Earth’s cross section to surface area.

did the impactor that killed the dinosaurs (57). Furthermore, we need a way to ensure, millions of years after the fact, that the material we have found has an extraterrestrial origin. Clearly the SN signal will be challenging to find and to confirm.

To confidently identify the origin of matter from nearby explosions, it must be distinguished from the terrestrial (or lunar) material surrounding it. This excludes stable isotopes that are the majority of SN ejecta, since these are abundant in Solar System material. However, live radioisotopes enjoy the great advantage of having little to no natural background, and thus radioactive species offer a means of tagging extraterrestrial material from recent nearby events. We can estimate the expected signal by computing the average surface density on Earth of a radioisotope i with mass number A_i , lifetime τ_i , and SN yield (ejected mass) $M_{ej,i}$. Accounting as well for efficiencies in transport f_i and sample incorporation efficiency (“uptake”) U_i , the number of atoms per square centimeter is

$$N_i = \frac{1}{4} U_i f_i \frac{M_{ej,i}}{4\pi A_i m_u D_{SN}^2} e^{-t_{SN}/\tau_i}, \quad 4.$$

$$N(^{60}\text{Fe}, 3 \text{ Myr}) = 2 \times 10^7 \text{ atoms cm}^{-2} U_{60} \left(\frac{f_{60}}{0.1} \right) \left(\frac{M_{ej,60}}{3 \times 10^{-5} M_\odot} \right) \left(\frac{50 \text{ pc}}{D_{SN}} \right)^2, \quad 5.$$

where Equation 5 is for $i = ^{60}\text{Fe}$ from an explosion 3 Myr ago, with fiducial parameter choices we discuss below. The overall factor of 1/4 represents the ratio of the Earth’s cross section to surface area. We see that the expected ^{60}Fe signal in Equation 5 (corresponding to $\sim 2 \times 10^{-15} \text{ g cm}^{-2}$) is significantly less than that of the main SN nucleosynthesis products, reflecting the small yields of intermediate-lived radioisotopes. Thus the background rejection achieved via radioactivity in turn demands highly sensitive techniques, favoring samples where the signal is concentrated and remains undisturbed.

Reference 60 showed that stable isotopes, or those long-lived enough to survive from the birth of the Solar System (such as ^{235}U), are lost to the terrestrial background. It also noted that SNe deliver radioisotopes of multiple origins: (a) the explosion ejecta, which generally dominate, but also (b) any interstellar radioactivity swept up by the blast, and (c) a “cosmogenic” component from the irradiation of Earth’s atmosphere by freshly accelerated cosmic rays. Focusing on the ejecta, it is clear from Equation 4 that favorable radioisotopes are those with the largest SN yields, and transport and geological considerations pose additional constraints.

Turning to the case of kilonovae, these events arise from neutron star collisions and are prolific sources of radioisotopes including the longest lived. The same basic formalism holds for kilonovae, the key difference being that the rates are much smaller. The neutron star merger rate is not measured precisely but is at most $\sim 1\%$ of the SN rate, making kilonovae within $\sim 100 \text{ pc}$ unlikely to occur within the lifetime of the Earth. But it remains possible that a kilonova can occur at a larger distance and, subsequently, a SN can sweep up its ejecta and deliver them to Earth in a two-step process.

3. RADIOISOTOPE PRODUCTION AND DELIVERY TO THE SOLAR SYSTEM

3.1. Radioisotope Synthesis in Supernovae and Kilonovae

The intermediate-lived radioisotopes we seek have lifetimes of ~ 1 to a few 100 Myr. Fortunately, nature has granted us an array of such isotopes, arising from a variety of nucleosynthesis processes and astrophysical sites. Here, we summarize the origins of a few key species (see **Table 1**); recent

Intermediate-lived radioisotopes:
lifetimes ~ 1 to $\sim 100 \text{ Myr}$ are long enough to survive transport but shorter than the Solar System’s age

Table 1 Selected radioisotope candidate signatures for nearby explosions

Isotope	Half-life $t_{1/2}$ (Myr)	Production site
^{26}Al	0.7	p capture: massive stars, CCSNe, cosmogenic background
^{53}Mn	3.7	NSE: CCSNe, SNIa, cosmogenic background
^{60}Fe	2.6	n capture: CCSNe
^{129}I	16.1	r-process
^{146}Sm	103	γ/p -process: CCSNe
^{182}Hf	8.9	r-process (s-process)
^{244}Pu	81	r-process
^{247}Cm	15.6	r-process

Abbreviations: CCSNe, core-collapse supernovae; NSE, nuclear statistical equilibrium; SNIa, supernova type Ia.

discussions of the whole set appear in References 63 and 64. Gamma-ray astronomy provides direct confirmation of ongoing astrophysical production of some of these species—nuclear lines are observed from the decays of ^{26}Al and ^{60}Fe (11, 30, 65, 66).

3.1.1. ^{60}Fe : supernova indicator. The ^{60}Fe isotope ($t_{1/2} = 2.62$ Myr) (67, 68) is neutron rich, and so its synthesis requires the presence of free neutrons. There must also be “seed” nuclei to absorb them—typically the stable ^{58}Fe isotope. The β decay of ^{59}Fe (which has a half-life of 45 days) competes with neutron capture, making this nucleus a branching point. The dominant origin of ^{60}Fe is thought to be core-collapse SNe, which are the endpoints in the evolution of massive stars $M \gtrsim 8\text{--}10 M_{\odot}$. There are several other likely sources of ^{60}Fe , but these generally are expected to make less of this isotope. Fortunately, we can use the observed ^{60}Fe , and the calculated explosion yields, to compare these sources and empirically determine which are the most likely.

Core-collapse SNe make ^{60}Fe both in the preexplosion hydrostatic phases and during the explosion; the ^{58}Fe seeds are preexisting material present at the star’s birth (30, 69–71). Production occurs via neutron captures of $^{58}\text{Fe}(n, \gamma)^{59}\text{Fe}(n, \gamma)^{60}\text{Fe}$, with destruction via $^{60}\text{Fe}(n, \gamma)^{61}\text{Fe}$ and $^{60}\text{Fe}(p, n)^{60}\text{Co}$. This mainly occurs in the He- and C-burning shells, in the late stages before the explosions and after it. The need to create neutrons, and competition for them with other neutron sinks, limits the ^{60}Fe production to be relatively low, with models giving ^{60}Fe yields roughly in the range of $M_{\text{ej},60} \sim (4 \times 10^{-6}\text{--}3 \times 10^{-4}) M_{\odot}$ (71–76). Winds prior to the explosions release very little ^{60}Fe , so most ^{60}Fe is ejected only by the SN outburst.

In addition to SNe, some ^{60}Fe may also be produced during helium burning in lower-mass stars ($M \sim 2$ to $9 M_{\odot}$) that undergo the asymptotic giant branch (AGB) phase. The yield is model-dependent and is related to the complexities of the dredge-up processes and winds in these pulsating stars. Recent estimates suggest this channel of Galactic production is relatively small (77, 78), but some individual events can have yields comparable with SNe.

Several other stellar sources of ^{60}Fe exist. Electron-capture SNe can produce up to $\sim 10^{-4} M_{\odot}$ of ^{60}Fe per event (79). These lie at the poorly determined lower-mass boundary for SNe, $\sim 8\text{--}10 M_{\odot}$, and could be rare today. Another potential source is from Type Ia SNe—the thermonuclear explosions of white dwarf stars. Most models predict that these have small ^{60}Fe yields (80), though rare Type Ia events may produce neutron-rich species including ^{60}Fe (81). Finally, neutron star mergers and the resulting kilonovae are unlikely to be significant sources of ^{60}Fe in our Galaxy (66).

3.1.2. ^{244}Pu : pure r-process. ^{244}Pu is unique in several ways. With a half-life of 81.3 Myr, it is among the longest-lived radioisotopes that do not have any remaining component from the birth of the Solar System. ^{244}Pu is also one of the heaviest known nuclei, and is highly neutron rich, with

56 excess neutrons. This points to an origin in an environment with a high neutron abundance. In fact, the microphysics of ^{244}Pu synthesis indeed calls for rapid neutron capture: the r-process (82, 83).

The basic nuclear physics of the r-process is well understood (84–86): A high neutron flux irradiates preexisting seed nuclei, creating neutron-rich species far from stability, all on a timescale of $\lesssim 1$ s. Subsequent decays populate stable and long-lived states. The r-process is the only mechanism known to produce actinides, including ^{244}Pu as well as ^{247}Cm ; these species thus unambiguously indicate r-process activity and probe its nature.

The r-process conditions clearly demand an explosive environment, and two sites are the main candidates: SN explosions and neutron star mergers. Supernovae were long thought to be the dominant site, as they broadly have the right characteristics of a dynamic site and a neutron-rich core. But as models have become more sophisticated, it has proven difficult to reproduce the solar r-process pattern with SNe (84, 86). Furthermore, SNe particularly struggle to make actinides, due to a lack of both sufficient neutrons per seed and neutrino environment around the proto-neutron star that suppresses neutron excesses. In many models SNe make no actinides and, thus, no ^{244}Pu at all! In addition, observations of r-process elements in the most primitive stars in our Galaxy, as well as in nearby dwarf galaxies, give insight into the population of r-process sources. These complex patterns are not consistent with a single r-process origin in any one source (87), but abundances of the heaviest species including actinides (which include ^{244}Pu) show variations that imply most SNe do not make these r-process species (85, 88, 89).

For these reasons, in the past two decades there has been increasing attention in the other potential r-process source: neutron star mergers (13, 90). The inspiral and collision of binary neutron star pairs leads to tidal tails and winds that eject neutron star matter at speeds of $v \sim c/4$. Models predict that as this material decompresses, it undergoes a vigorous r-process that may include actinide production (12, 86). As the newborn r-process material decays toward stability, the energy release powers an electromagnetic display that marks a kilonova event. This basic scenario has strong observational support from the kilonova observations associated with the neutron star merger gravitational-wave event GW170817. The observed luminosity time history (light curve) and spectra are consistent with a robust r-process and the ejection of $\sim 10^{-4}$ to $10^{-3} M_{\odot}$ of material, although the available data do not directly unveil the details of the nucleosynthesis pattern in that event (15, 91).

It is thus clear that neutron star mergers/kilonovae contribute significantly to the Galactic r-process inventory today and could be the dominant source. But it remains an open question how much SNe contribute to the r-process and whether some SNe produce actinides (92). For example, SN models that created magnetohydrodynamic jets, or rapidly rotating massive stars giving rise to “collapsars,” do undergo an r-process that can yield ^{244}Pu and other actinides (though collapsars are less likely to occur in the modern, metal-rich Milky Way) (93–98). These SNe are expected to be rare but could provide a way to produce ^{244}Pu and the rest of the r-process along with ^{60}Fe . Confirming that such events occur in nature would have important consequences for the r-process and for heavy element production in the cosmos generally.

An important distinction between the SN and kilonova production of actinides is that in general the SN models struggle to reach the actinide region while making much more of the lighter r-process species, including radionuclei such as ^{129}I . By contrast, the kilonova models robustly produce actinides and go on to initiate fission, leading to a fission cycling equilibrium between actinides and lighter r-process species. This means that the ratio of radioisotopes such as $^{129}\text{I}/^{244}\text{Pu}$ are signatures of the nature of actinide nucleosynthesis; measurement of multiple r-process radioisotopes thus promises to offer a unique and sharp probe of the r-process site and mechanism (64).

3.1.3. Other radioisotope messengers. In addition to ^{60}Fe , SNe produce other intermediate-lived radioisotopes. We summarize these here; more details of their nucleosynthesis pathways were recently summarized in Reference 76. If multiple SN species are detected from the same event, this can allow determination of the SN mass and probes the details of the burning processes as well as transport properties discussed in the next sections.

SNe produce ^{26}Al and ^{53}Mn via proton capture, with yields of $M_{\text{ej}} \sim \text{few} \times 10^{-5} M_{\odot}$, which is comparable with ^{60}Fe (69, 72). Heavier SN radioisotopes have substantially smaller abundances, typically on the order of $M_{\text{ej}} \sim 10^{-9} M_{\odot}$, and so would be more challenging to detect (76). The neutron-rich ^{129}I , ^{135}Cs , ^{182}Hf , and ^{205}Pb are formed by neutron capture on preexisting seed nuclei in ordinary hydrostatic and explosive burning (in addition to any r-process production around the proto-neutron star). The proton-rich species ^{146}Sm , ^{97}Tc , and ^{98}Tc are produced largely by the γ process of photodisintegration of heavier species.

Turning to the r-process, this mechanism makes a wide array of intermediate-lived radioisotopes. As noted in the previous section, kilonova models give a robust r-process that makes all species including actinides. But it remains unproven whether SNe can produce the r-process at all, and it is particularly challenging for SNe to produce actinides. Thus, the ratios of ^{244}Pu to other r-process radionuclides make for particularly powerful diagnostics. Because SNe only barely reach the actinide region, they should have much higher ratios of lighter species to ^{244}Pu ; these include ^{93}Zr , ^{107}Pd , ^{129}I , and ^{182}Hf . For example, production ratios (after 0.1 Myr) for two different models each for SNe and kilonovae give (64)

$$\left(\frac{^{129}\text{I}}{^{244}\text{Pu}}\right)_{\text{SN}} = 7.1 \times 10^2 \text{ to } 4.5 \times 10^6 \quad \text{and} \quad \left(\frac{^{129}\text{I}}{^{244}\text{Pu}}\right)_{\text{KN}} = 41 \text{ to } 180. \quad 6.$$

The large ratios in the SN case reflect their difficulty in producing actinides, and the large range reflects a strong model dependence as well as nuclear physics uncertainties. On the other hand, the kilonova ratios are smaller, and they cover a much narrower range determined mostly by nuclear physics uncertainties. We see that measurements of ^{129}I , ^{182}Hf and similar light r-process species could distinguish these two cases despite the nuclear uncertainties.

It is also noteworthy that for SN models that make actinides, the ratios among isotopes *within* this group are similar to the ratios in kilonova calculations. Thus, both SN and kilonova models make similar predictions for the ratios of ^{247}Cm , ^{237}Np , and ^{236}U relative to ^{244}Pu . This means that because ^{244}Pu has been detected, these other species should also be present, in amounts that are relatively well-determined (64). These species thus serve as a consistency check of the basic r-process physics.

3.2. Radionuclides After the Explosion: Incorporation of Interstellar Dust and Cosmic Rays

Once a nearby SN or kilonova explosion produces radioisotopes, they must be delivered to us in order to be observable. We divide this journey into two steps. In this section, we consider propagation in the explosion remnant that engulfs the Solar System. In the next section, we turn to propagation within the heliosphere to reach the Earth and Moon.

Consider first the simplest case of an isolated SN explosion, embedded in the interstellar medium (ISM). Relatively rapidly, the hot gas in the blast sweeps up a mass of interstellar gas comparable with the ejecta mass and then forms a thin shell enclosing a hot and rarefied interior. This basic structure persists as the remnant expands and sweeps up more matter. Conservation of energy and momentum leads the blast to slow as it grows. Finally at late times up to ~ 1 Myr and sizes of ~ 100 pc, the supersonic shock wave slows to become a sound wave, and the blast “fades away” to become part of the ISM (99).

Within the SN remnant, the ejecta take two forms. The bulk of the ejecta is gas (plasma) dominated by hydrogen and helium. The gas phase also dominates for heavy elements having a low condensation temperature—“volatile” species such as nitrogen and argon. In contrast, “refractory” elements that have a high condensation temperature can form microscopic solids—*dust grains*. Dust is observed in young SN remnants (100), and SN dust seen as presolar grains in meteorites confirm both that grains form rapidly and that some survive the remnant (101).

Iron, plutonium, and most of the elements hosting intermediate-lived radioisotopes are refractory, and so we expect some of the SN yields of these species to be locked into dust grains. In the next section, we show that these grains play a crucial role in radioisotope delivery to the Earth. Dust is also a major constituent of the heavy element component of the ISM of the Milky Way and other galaxies, and the role of SNe in producing and destroying dust is a subject of intense research (102) for which live ^{60}Fe and ^{244}Pu detections provide important new information.

Supernova blasts are also the engines of cosmic-ray acceleration (103), most likely via shock acceleration (104). The elemental composition of cosmic rays shows enhancements in refractory species, implying that species in dust are preferentially incorporated into cosmic rays. Reference 105 argues that this fits into a picture in which dust grains undergo mild acceleration in supernovae, with sputtered elements forming the seed population for heavy elements in cosmic rays. Sputtered grains from the supernova might be the origin of ^{60}Fe detected in cosmic rays (28). On the other hand, grains surviving the supernova can eventually lead to radioisotope deposition on the Earth and Moon.

We turn now to the blasts of kilonovae, which are rarer than SNe and not well understood. The total kinetic energy for the kilonova seen with GW170817 is estimated at $E_{\text{kin}} \sim (1 - 2) \times 10^{51}$ erg (91), comparable to the value for a typical SN. Given the similar explosion energies, some of the kilonova remnant features and evolution will broadly remain the same as in SN remnants—including supersonic shock wave, and a swept-up shell. But the kilonova ejecta have lower mass and higher speed, and are likely significantly anisotropic, so that some of the blast features and evolution can be different in detail (106). It is also unclear whether dust grains are able to form in the high-speed kilonova ejecta (107, 108).

3.3. Transport Into the Solar System: Supernovae and Interstellar Medium Models

Upon reaching the Solar System, the radioisotope-laden SN blast encounters the outward flow of the solar wind. This wind–wind collision reshapes the heliosphere—the domain of the unperturbed solar wind—from its present configuration, which extends to ~ 100 AU today. This compressed heliosphere is the arena in which SN debris—including radioisotopes—must be brought to the Earth and Moon.

An order-of-magnitude calculation illuminates the key question of how SN debris reaches the Earth. The solar wind at our 1-AU location has a proton number density of $n_p \sim 10 \text{ cm}^{-3}$ and a speed $v_{\text{sw}} \sim 400 \text{ km s}^{-1}$, which gives a ram or dynamic pressure $P_{\text{sw}}(1 \text{ AU}) = m_p n_p v_{\text{sw}}^2 \sim 2 \times 10^{-8} \text{ erg cm}^{-3}$. A SN blast at distance D_{SN} has pressure $P_{\text{SN}} \sim E_{\text{SN}}/D_{\text{SN}}^3$. Using a SN energy $E_{\text{SN}} = 10^{51}$ erg, we find that momentum (i.e., pressure) balance $P_{\text{SN}} = P_{\text{sw}}$ occurs for a SN distance $D_{\text{SN}} \sim 10 \text{ pc}$. That is, for SN gas to reach 1 AU, the explosion must be very close—indeed, at the kill distance! A more common nearby SN at a larger distance will not reach the Earth and Moon.

This conclusion is borne out in detailed calculations: **Figure 2** shows the heliospheric response to a SN at $D_{\text{SN}} = 63 \text{ pc}$ (109), which is a plausible distance to the SNe detected with ^{60}Fe . We see that the closest approach of SN material is about 25 AU—much closer than the heliospheric boundary today but far from the inner Solar System. Only the rare lethal SN can directly deliver

Astronomical unit (AU): the average distance between the Earth and the Sun;
 1 AU = $1.5 \times 10^{13} \text{ cm} = 5 \times 10^{-6} \text{ pc}$

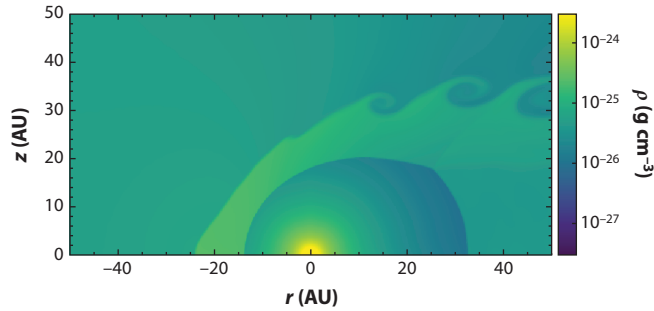


Figure 2

Simulation of a SN blast colliding with the solar wind, for an explosion 63 pc away. The Sun is located at the origin, and the SN blast is a plane wave moving from left to right; cylindrical coordinates are shown in astronomical units, and axisymmetry is enforced. In this map of gas density, we see the heliosphere region of the solar wind is violently compressed, with the SN’s closest approach around $z = -25$ AU, at the heliopause discontinuity. Note that the SN gas (plasma) does not reach Earth’s orbit at 1 AU (*bottom center*). Abbreviation: SN, supernova. Figure adapted from Reference 109.

gaseous ejecta to Earth, while more common events—including those responsible for the ^{60}Fe pulses—cannot (109, 110).

How can ^{60}Fe arrive at Earth if the SN gas does not? The key is that some of these refractory elements are in the form of dust grains (111). When dust in the SN blast encounters the solar wind, the fast micron-sized grains decouple from the gas and travel through the solar wind, reaching the Earth and Moon (111–113).

Thus, we see that to reach Earth, SN radioisotopes must be in the form of dust grains. Fortunately, most intermediate-lived radioisotopes—including Fe and Pu—should readily form dust grains. But not all such atoms go into dust, and the harsh environment of the SN remnant can destroy some grains. We account for these losses via an efficiency factor f_i giving the fraction of SN mass in i that can arrive at 1 AU. This “dust fraction” is not well known but estimates are around $f_i \sim 1\%$ to 10% (114). We see that the detection of radioisotopes on Earth is tied up with the astrophysics of SN dust.

Having delivered newly synthesized radioisotopes to Earth, it remains to be determined where and how to detect them. We now turn to these questions.

4. DETECTION METHOD: ACCELERATOR MASS SPECTROMETRY

The ^{60}Fe fluence in Equation 5 arrives over ~ 1 Myr, leading to deposition rates into terrestrial archives on the order of atoms per square centimeter per year. For ^{244}Pu , this drops to a few atoms per 100,000 years. Only the most sensitive methods are able to detect these minute amounts of interstellar signatures. The most sensitive techniques for identifying longer-lived radionuclides are direct atom counting techniques, in particular AMS (115–117). While in principle other techniques have also demonstrated high measurement sensitivity (118, 119) or also high selectivity (120), only AMS has been successful in detecting traces of interstellar radionuclides in terrestrial or lunar archives.

AMS is a mass spectrometric technique that is able to identify radionuclides at their natural abundances, which can be 10 to 17 orders of magnitudes lower than the stable (terrestrial) isotope (e.g., radionuclide ^{60}Fe versus stable Fe) (117, 121). Different than other mass spectrometric techniques, the use of an accelerator allows complete suppression of any interfering background molecules of the same mass from the beam (115–117).

AMS provides high measurement selectivity and sensitivity and is able to detect single atoms. This capability requires efficient suppression of background ions and a high measurement efficiency for the rare isotope. The major background sources in AMS are interferences by isobars (particles with the same mass) and isotopes (particles of the same element, but different mass) many orders of magnitude more abundant. Isobaric interferences can be reduced by dedicated chemical purification protocols, by destroying molecules of the same mass, and finally by particle identification techniques in a final particle detector. Isotopes cannot be separated by dedicated chemical treatments but must be removed from the ion beam by mass-selective processes (mass filters) during the ion transport, sometimes combined with high-resolution energy (or velocity) measurements by particle detectors.

Owing to the high particle energies provided by the accelerator, the radionuclides can be identified via nuclear physics-based particle detection methods. Isobaric background suppression improves with particle energy, thus large accelerators providing high particle energies are often necessary; this is especially the case for ^{60}Fe detection (121, 122). By contrast, ^{244}Pu has no stable isobar (note, molecules are completely destroyed in AMS), thus it faces background from isotopic interference only. However, because of the low content of ^{244}Pu in a sample, the highest measurement efficiencies are mandatory (see below).

A simplified schematic of an AMS system appears in **Figure 3**. In the following, we trace the path of a sample through this system, from preparation to final detection.

4.1. Sample Preparation: Separation, Purification, and Element Enrichment

The main aim in sample preparation is to separate, purify, and enrich the isotope of interest for a measurement. The radionuclide concentration in the measurement sample is accordingly

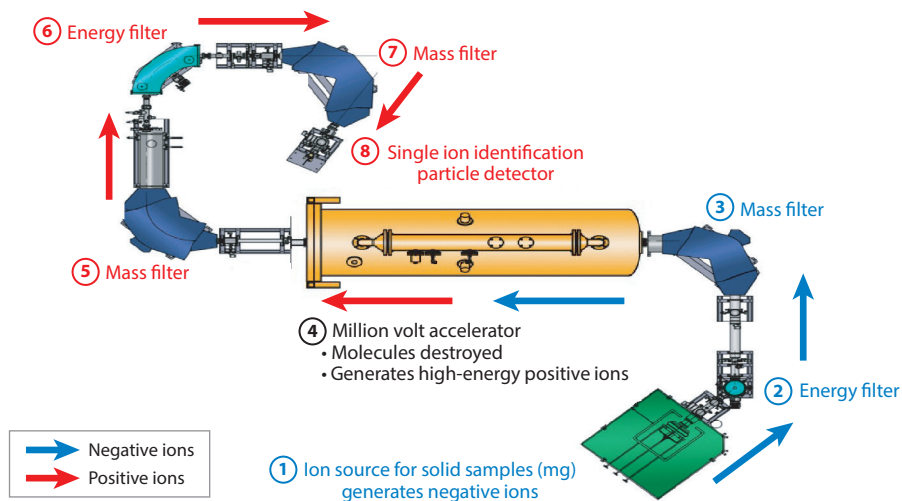


Figure 3

Simplified schematic of an accelerator mass spectrometry system, with blue arrows indicating negative ion trajectories and red arrows positive (highly energetic) ion trajectories. Samples with mass of a few milligrams are slowly consumed and negative ions are extracted from the ion source. After energy and mass filtering, the ions are injected into a particle accelerator. Here, negative ions are accelerated to high energies ($\sim 1\text{--}100\text{--MeV}$ energy). Stripping off electrons produces positive ions for further acceleration, and molecules will split into their individual constituents. High-energy mass and energy filters remove further background before the individual ions are counted one by one in the final particle detector.

increased by orders of magnitude: If a deep-sea crust sample contains ~10% Fe, then a pure Fe sample yields a factor of 10 enrichment; selective leaching procedures of Fe in a sediment may lead to enrichment factors greater than 100 (123). Still, spurious amounts of other elements at the per-mille to ppm level may remain, which in the case of isobars may be the limiting factor in measurement sensitivity.

^{244}Pu , having no stable Pu isotopes, is embedded into a matrix of a different element, often Fe powder. In this way, e.g., Pu can be extracted from a 100-g sample and recovered within 1 mg Fe, which means an enrichment by a factor of 10,000 to 100,000.

4.2. Ion Production, Ion Transport, and Single-Atom Counting

AMS identifies single ions and counts them one by one. This process involves several steps from ion production to background filtering and final particle detection.

- **Ion production:** **Figure 3**, step 1. A few milligrams of processed sample material is slowly consumed in an ion source by sputtering the sample at rates on the order of milligrams per hour. A fraction of the sputtered atoms become negatively charged and can be extracted and accelerated away from the ion source.
- **First low-energy filtering:** **Figure 3**, steps 2 and 3. The negative ions are then filtered in mass, energy, and charge by electrostatic and magnetic deflectors. Still present in the beam are—besides the isotope of interest—isobars and some small fraction of residual background ions. While conventional low-energy mass spectrometers would at this stage measure the ion beam intensity, AMS applies additional filtering elements that improve the measurement sensitivity by several orders of magnitude.
- **Particle acceleration and molecule destruction:** **Figure 3**, step 4. After the low-energy filtering, the beam is sent toward an accelerator producing on the order of million-electronvolt particle energies, which is typical for nuclear physics applications. Stripping off electrons produces positive ions where molecules become unstable and consequently split into their constituents.
- **High-energy mass filter:** **Figure 3**, steps 5–7. The now positively charged high-energy particles must pass another magnet that selects a certain combination of mass, energy, and charge state. This removes the molecule fragments whose constituents have lower masses than the radionuclide.
- **Final ion identification in a particle detector:** **Figure 3**, step 8. The ions of interest are finally counted one by one with a particle detector. A fraction of background ions may still also enter the detector and must be identified against the rare isotope. Such particles can be isobars or tails of neighboring isotopes and some scattered particles or other ions that are not completely filtered away. The ions are stopped in the detector, and their energy loss in this stopping process is characteristic for a specific element.

Isobar suppression becomes more efficient for particles having a higher initial energy. Therefore, ^{60}Fe detection requires sufficient particle energy that is only provided by the largest tandem accelerators used for AMS. Presently, only one facility exists that provides the required sensitivity to detect interstellar ^{60}Fe (see the sidebar titled Accelerator Mass Spectrometry of ^{60}Fe).

A different situation exists for the second interstellar isotope, ^{244}Pu (see the sidebar titled Accelerator Mass Spectrometry of ^{244}Pu). In contrast to ^{60}Fe , Pu does not have any stable isobars that need to be separated; rather, neighboring isotopes need to be removed efficiently. Most important here is the abundance sensitivity, considering the fact that interstellar ^{244}Pu is many orders

ACCELERATOR MASS SPECTROMETRY OF ^{60}Fe

A typical sample for AMS consists of a few milligrams of powder. An Fe-oxide sample is prepared and pressed into a sample holder. A 5-mg sample contains $\sim 5 \times 10^{18}$ ^{56}Fe atoms, which at a ratio of $^{60}\text{Fe}/\text{Fe} \sim 5 \times 10^{-16}$ corresponds to $\sim 25,000$ ^{60}Fe atoms. A fraction of 2×10^{-4} ions in the sample will eventually be transmitted and identified with the particle detector (35, 68, 121), which is equivalent to yielding about five detector events for this sample. Such a sample would last for several hours of measurement before it is fully consumed, i.e., sputtering rates in the ion source are on the order of milligrams per hour. Accordingly, the ^{60}Fe count rate measured with the particle detector will be ~ 1 event every one or two hours for this example.

The stable isobar to ^{60}Fe is ^{60}Ni . Despite the best efforts of the chemist, its relative abundance in the AMS sample will still be at a ppm (10^{-6}) level, meaning ^{60}Ni is 9 to 10 orders of magnitudes more abundant. If sent unattenuated to the detector, its intensity would completely overwhelm the detector with $\sim 1,000,000$ particles per second. Thus, the ^{60}Ni beam intensity needs to be reduced before entering the detector, e.g., by the use of a gas-filled magnet, which spatially separates the ^{60}Ni from the ^{60}Fe beam (20, 121).

of magnitude less abundant than the rare ^{60}Fe . This is best achieved today with dedicated smaller AMS systems (124, 125).

5. MEASURED RADIONUCLIDES IN DEEP-SEA AND LUNAR ARCHIVES

Interstellar messengers of recent cosmic nucleosynthesis events comprise the direct detection of interstellar radionuclides in geological archives (the topic of this section) and additional samples of extraterrestrial origins (cosmic rays, meteorites, stardust grains), as well as the many astronomical observations. For a recent review, see Diehl et al. (66).

Both ^{60}Fe and ^{244}Pu are perfect candidates for the search of interstellar signatures in terrestrial and lunar archives:

- Both were present at the time of Solar System formation, but owing to their short half-life compared to the age of the Solar System, both are essentially extinct now.

ACCELERATOR MASS SPECTROMETRY OF ^{244}Pu

^{244}Pu , having no stable isotopes, is typically extracted together with another Pu isotope, usually ^{242}Pu , which is added as a measurement tracer and allows monitoring of chemical yields. The final Pu-AMS sample is Pu embedded in another matrix element, usually an ~ 1 -mg Fe powder mixed with other metals to improve negative formation in the ion source. The AMS ratio $^{244}\text{Pu}/^{242}\text{Pu}$ allows calculation of the number of ^{244}Pu atoms in the sample because the number of ^{242}Pu added is known. A fraction of 10^{-2} Pu ions in the sample will eventually be transmitted and identified with the particle detector (125).

AMS of ^{244}Pu is background-free, meaning that no detector event will be registered over several hours of measurement time. If we require five detector events for a significant signal, at least 500 ^{244}Pu atoms need to be present in the sample. If these ^{244}Pu atoms were extracted from a 100-g sample, atom concentrations of $< 10^{-21}$ ^{244}Pu atoms per atom in the archive can be detected; this means ^{244}Pu -AMS is sensitive at the zepto-scale level. Such a “Pu-sample” would last for more than five hours of measurement before it is fully consumed. Accordingly, the ^{244}Pu count rate measured with the particle detector will be ~ 1 event every 1 or 2 hours for such a sample.

- The high neutron densities required for their production prevent natural production of ^{60}Fe and ^{244}Pu on Earth in significant amounts.
- Live ^{60}Fe on Earth indicates nearby SN activity within the past ~ 10 Myr.
- ^{244}Pu present on Earth indicates r-process nucleosynthesis within the past few 100 million years. Influx of ^{244}Pu can help to identify the site for the heavy r-process.
- Finally, AMS can measure both ions with high sensitivity or nearly background-free.

The influxes (terrestrial fluence) of ^{60}Fe were shown to be distributed over time periods of several 100,000 to million years with distinct peak-like time profiles.

5.1. Archives and Terrestrial Deposition

Once the interstellar particles have arrived at the Moon or Earth via ISM dust grains as transport vehicles, they either will be implanted into the lunar surface or will rain down onto Earth (113). In the latter case, the dust grains ablate and vaporize, i.e., the nuclides are released from the grain within the atmosphere. Eventually these particles are deposited on land or the ocean, where they take part in geological processes in the same way as their terrestrial isotopic counterparts.

Interstellar particles can accumulate over millions of years in deep-ocean archives and in lunar soil, imprinting isotopic fingerprints. Lunar soil integrates over timescales of some ten to hundred million years. In contrast, Earth's surface faces continuous change. Soil movement, erosion, etc., redistributes material over large volumes; i.e., an interstellar signal will be diluted before it decays away. Geological archives can retain the temporal signal if they grow undisturbed over long time periods. In the following, we discuss deposition into various archives for the two most prominent radionuclides, ^{60}Fe and ^{244}Pu , in more detail.

Proper geological archives include ice cores, deep-sea sediments, and crusts. Antarctic ice cores record time periods of a few 100,000 years (126), whereas deep-sea sediments and ferromanganese crusts (FeMn crusts; see **Figure 1**) and nodules grow over millions of years (127, 128). They all allow a retrospective search of interstellar influx onto Earth. Lunar soil has no definite growth pattern because the top surface is continuously reworked by the bombardment of interplanetary particles such as (micro) meteorites and possibly interstellar particles over long time periods.

In the following, we assume that the interstellar particles are distributed homogeneously across the globe. Here, we neglect that local atmospheric disturbances and latitudinal effects might lead to variations in their deposition. Similarly, the complex thermohaline circulation of the ocean might transport the extraterrestrial nuclides away from the location where they arrived at the ocean surface (113).

Different geological archives grow at different rates. 1,000 years of accumulation in an ice core corresponds to ~ 10 m of sample length, while the same integration time will be only a few millimeters in a deep-sea sediment. Finally, even more compact archives are deep-sea crusts or nodules with a growth rate of a few micrometers in 1,000 years.

The incorporated radionuclide concentrations are a function of the archive's growth rate. We discuss the expected deposition for two cases, where the interstellar signal is extended in time over 10,000 and 1,000,000 years. This corresponds to an average terrestrial ^{60}Fe particle flux of 2,000 and 20 ^{60}Fe atoms per square centimeter and year, respectively (see the sidebar titled Expected Concentrations of ^{60}Fe and ^{244}Pu in Geological Archives).

Note that sampling of individual layers representing 10,000 years is possible for sediments (a few centimeters sample length) but not for deep-sea crusts, where the experimental limit for an individual layer is at best fractions of millimeters; i.e., time resolution in a crust will be limited to some 100,000 years per individual layer.

EXPECTED CONCENTRATIONS OF ^{60}Fe AND ^{244}Pu IN GEOLOGICAL ARCHIVES

^{60}Fe concentrations are 10^2 – 10^5 ^{60}Fe atoms g^{-1} sediment (10^{-17} – 10^{-19} $\text{g } ^{60}\text{Fe g}^{-1}$ sediment) and 10^6 – 10^7 ^{60}Fe atoms g^{-1} crust (10^{-15} – 10^{-17} $\text{g } ^{60}\text{Fe g}^{-1}$ crust). Here, we took into account that a deep-sea crust incorporates Fe arriving at its surface with efficiency $U_{\text{Fe,crust}} \sim 10\%$ (for terrestrial and interstellar Fe). In contrast, ice cores and sediments are assumed to take up 100% of the arriving particles.

^{60}Fe is measured with AMS as an isotope ratio; i.e., ^{60}Fe is counted relative to the stable terrestrial Fe in the archive. With a stable Fe content of a few % (deep-sea sediments) and up to 20% (crusts), we find isotopic ratios of interstellar ^{60}Fe relative to terrestrial Fe, $^{60}\text{Fe}/\text{Fe}$, of $\sim 10^{-15}$ or less for both archives for a signal distributed over a time period of one million years. Only in the case of the short-term influx scenario of 10,000 years would the signal be condensed within a few centimeters of sediment, and the isotope ratio would scale accordingly with $^{60}\text{Fe}/\text{Fe}$ up to 10^{-13} .

For ^{244}Pu a much lower influx is expected, yielding concentrations on the order of 10^{-20} ^{244}Pu atoms per crust atom or lower (see above), i.e., sensitivities at the zepto scale. For other interstellar candidates, such as ^{53}Mn and ^{26}Al , nucleosynthesis yields and consequently concentrations in the terrestrial archive would be of similar magnitude as ^{60}Fe (assuming similar transport and incorporation efficiencies).

We note, micrometeorites (and meteorites) would also transport continuously some cosmogenically produced ^{60}Fe to Earth, which has its origin in the Solar System, and this had been suggested as another source for the observed ^{60}Fe influx (129, 130). It had been shown that the measured ^{60}Fe influx is much higher than expected from any interplanetary ^{60}Fe source (22–24, 131). Furthermore, recent ^3He measurements (with dominant production in the Solar System) found no ^3He – ^{60}Fe correlation in the same deep-sea sediments that showed ^{60}Fe excess in support of its interstellar origin (132).

Owing to continuous growth over time, sediments and crusts exhibit a depth-age correlation. Layers can be dated by taking advantage of the natural decay of radionuclides in the archive. The best-suited radionuclide is ^{10}Be , with a half-life of $t_{1/2} = 1.387$ Myr (133; see also 128 and 131), which is produced naturally in Earth's atmosphere. Another nuclide for dating would be cosmogenic ^{53}Mn ($t_{1/2} = 3.7$ Myr). It would allow for a longer dating range, but this nuclide is more difficult to measure (36).

5.2. ^{60}Fe Measurements: Supernova Detections

The ^{60}Fe influx observed on Earth could originate from different sources (see discussion in Section 3.1.1), such as (a) high-energy cosmic ray particles; (b) cosmogenic ^{60}Fe , produced within the Solar System by nuclear reactions (spallation) induced by cosmic rays and deposited through micrometeorites raining down on Earth; and finally (c) nuclides, freshly produced in stars, ejected into space and transported to Earth via interstellar dust grains. The first two components are negligible for ^{60}Fe , as is natural production on Earth.

Various archives have been studied for signatures of interstellar ^{60}Fe . In particular, the group at the Technical University of Munich (TUM) pushed the limits in background suppression to achieve the required sensitivity for detection of interstellar ^{60}Fe . Based on their large 14-MV Emperor (MP) tandem accelerator, this group pioneered this research in the late 1990s (20, 21). The AMS group of Australian National University (ANU) Canberra developed the AMS technique at their 14-MV Pelletron tandem accelerator as well (68). This is now the only such facility since TUM shut down its activities in 2020. The AMS group at ANU reports for ^{60}Fe a

COUNTING ATOMS WITH AMS

AMS counts individual atoms of rare isotopes. Over the past ~20 years, the total number of interstellar ^{60}Fe atoms detected in all samples to date is around ~1,500, most of which were found in the latest measurements in the last few years where efficiencies were the highest. For ^{244}Pu a higher detection efficiency somewhat offsets the lower abundances, yielding so far a total of ~190 counts above background—with only six detector events, which is compatible with anthropogenic sources, prior to 2021.

measurement background of $^{60}\text{Fe}/\text{Fe}$ as low as 3×10^{-17} (35, 121), which is equivalent to about one ^{60}Fe background event over 1 day of measurement.

Interstellar ^{60}Fe has been detected so far in nine different deep-sea FeMn crust samples (20–24, 134), six different deep-sea sediment cores (23, 135, 136), and two deep-sea nodules (23), as well as in lunar soil samples from three Apollo missions (27) and in Antarctic snow (26). Interstellar ^{60}Fe was found in a biogenic reservoir (fossilized magnetotactic bacteria in deep-sea sediments) (136). Both groups used AMS for these measurements (see the sidebar titled Counting Atoms with AMS).

Figure 4 shows an extensive set of AMS data from deep-sea sediments, crusts, and nodules. Plotted are isotope ratios $^{60}\text{Fe}/\text{Fe}$ with ^{60}Fe assumed to be interstellar and stable Fe assumed to be terrestrial. This ratio is a function of the stable Fe content in the archive and may depend also on the chemical extraction efficiencies in the sample preparation (e.g., when leaching to extract authigenic Fe), which can modulate the absolute scale of the final isotope ratio. However,

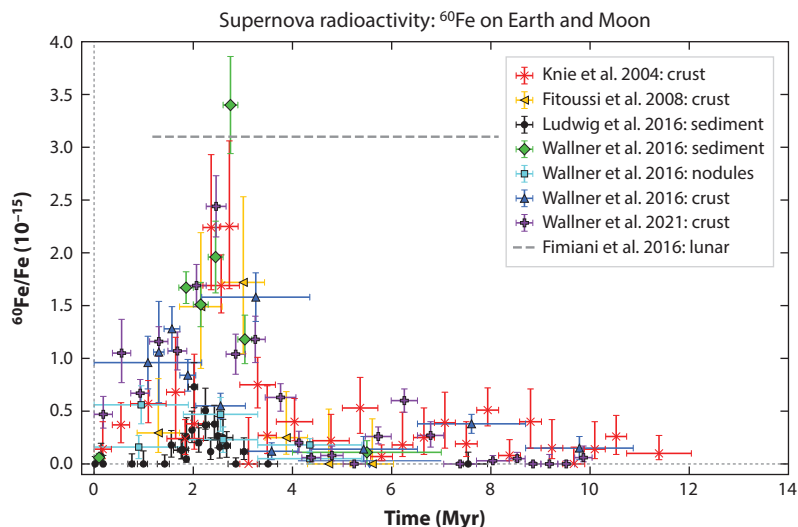


Figure 4

Summary of terrestrial and lunar data on ^{60}Fe . Measured $^{60}\text{Fe}/\text{Fe}$ isotope fractions are shown without correction for decay. All measurements show a pulse ~2–3 Myr ago (SN Plio), while References 23 and 24 find for two crust samples a second pulse at ~6 to 7 Myr ago (SN Mio). Abbreviations: SN Mio, Miocene supernova; SN Plio, Pliocene supernova. Data from References 21–24, 27, and 136. Figure adapted from Reference 25.

when comparing different archives and measurements of different groups one should focus on the relative shape of the temporal influx pattern as this will not be affected. The data show that ^{60}Fe was found in all major oceans, demonstrating that the ^{60}Fe signal is a global signal; ^{60}Fe influx is extended in time and must be of interstellar origin from multiple events, as no other sources are known to explain this influx. Two broad signals point to long-term influxes of ^{60}Fe , possibly caused by several close-by SN explosions. The measurement background for the most recent data (since 2016) corresponds to a ratio $^{60}\text{Fe}/\text{Fe}$ of 0.03×10^{-15} , i.e., a ratio that is negligible for the two peaks in influx; for the earlier measurements the background was assumed to be $^{60}\text{Fe}/\text{Fe} \sim 0.2 \times 10^{-15}$.

The general time profile of the ^{60}Fe influx is reproduced in all archives: It peaks at about 2.5 to 3 Myr before present and continues throughout the Holocene (evidenced in modern deep-sea sediments) (135) until present (as evidenced in modern Antarctic snow) (26). Sediments show influx rates of up to ~ 40 atoms $\text{cm}^{-2} \text{ year}^{-1}$ (23), but are reduced to between one and a few atoms per square centimeter per year in recent times.

The crust data provide a time profile beyond the 5 Myr covered by sediment data. Overall, no significant influx was observed between 4 and 5.5 Myr ago, but a significant second influx was detected between 6 and 8 Myr in two crust samples (23, 24). A continuous record of individual ^{60}Fe data is plotted for a crust sample from the Pacific Ocean in **Figure 5a**. Here, a time period of 10 Myr is covered, where single data points represent 1 mm of crust, which is equivalent to a coverage of $\sim 300,000$ years per layer. These data have been converted into ^{60}Fe deposition rates into the crust sample. The same crust was also used for parallel ^{244}Pu measurements (see below) (24).

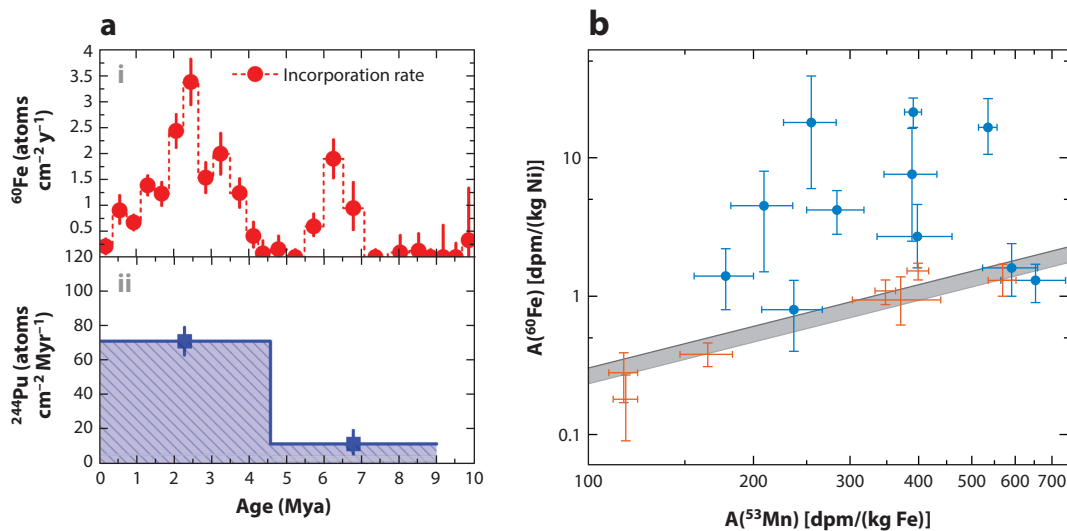


Figure 5

(a) Multiple radioisotope species detected in a deep-ocean FeMn crust spanning the past 10 Myr. (i) ^{60}Fe flux, showing two clear peaks, one at ~ 7 Mya (SN Mio) in addition to a confirmation of the peak around 3 Mya (SN Plio). (ii) ^{244}Pu flux showing the presence of this r-process species in the same time window. Note the change in scale in the vertical axes from atoms per square centimeter per year for ^{60}Fe to atoms per square centimeter per million years for ^{244}Pu , respectively. Panel adapted with permission from Reference 24.

(b) Detection of extraterrestrial ^{60}Fe on the Moon. Specific activity shown in decays per minute per kilogram measures radioisotope atoms per gram of cosmic-ray target. Meteoritic data (*crosses*) follow expected correlation for cosmic-ray production of ^{60}Fe and ^{53}Mn (*thick gray band*). Apollo lunar regolith samples (*solid points*) do not follow this trend, showing an excess in ^{60}Fe . Reference 131 gives more details on the ^{53}Mn – ^{60}Fe correlation. Panel adapted with permission from Reference 27. Abbreviations: SN Mio, Miocene supernova; SN Plio, Pliocene supernova.

We can estimate the total ^{60}Fe interstellar fluence from the sediment data as published in Reference 23 with the assumption of 100% incorporation and a homogeneous distribution across Earth's surface. Using the crust data to include the time period not covered by sediments, we find $\sim 1.5 \times 10^8$ ^{60}Fe atoms cm^{-2} arrived at Earth orbit during the past 4 Myr and for the older peak $\sim 1/3$ of this, $\sim 0.5 \times 10^8$ ^{60}Fe atoms cm^{-2} (23, 24, 135). This can also be compared to the lunar data in **Figure 5b**, which suggest some $0.8\text{--}4 \times 10^8$ ^{60}Fe atoms cm^{-2} arrived at Earth's orbit (27).

From the ^{60}Fe data, one can conclude that Earth was exposed to SN ejecta, or alternatively the Solar System could also have moved through clouds of ^{60}Fe -enriched dust. The lunar detection confirms that the signal reached the entire inner Solar System and is thus extraterrestrial.

5.3. ^{244}Pu Measurements: r-Process Detection

Detection of ^{244}Pu is even more challenging because the expected influx would be much lower compared to ^{60}Fe —if SNe produce actinides at all (see Section 3.1.2). An archive might also contain additional older ^{244}Pu from the ISM.

Thanks to the extraordinary improvement in detection efficiency for actinide-AMS in the past decade (124, 125), searches for extraterrestrial ^{244}Pu have become feasible in recent years. Dedicated systems quote now a detection efficiency for Pu of $>1\%$ (125), about a factor of 100 better than the present detection efficiency for ^{60}Fe . This partly compensates for the about 4 to 5 orders of magnitude of lower deposition rates compared to ^{60}Fe .

Parallel to that for ^{60}Fe , the AMS technique for detection of interstellar ^{244}Pu was also developed, at the Hebrew University (137, 138) and at TUM (139, 140). First results confirmed low influx values, however, giving only upper limits.

About 10 years later and using the same crust that showed the first clear ^{60}Fe peak (237KD) (21), but with ^{244}Pu extracted from kilogram samples of material, new measurements at the University of Vienna produced limits that were much lower than expected from regular r-process production of ^{244}Pu in SNe (37). However, these and previous data were based on detections of only one or two events (^{244}Pu events registered with the detector).

A clear signal of ^{244}Pu , well above anthropogenic production, was found only recently (24) owing to the improved detection sensitivity. ^{244}Pu is thus the second radionuclide for which a significant interstellar signal has been observed in terrestrial archives. The measured ^{244}Pu fluence is consistent with the previous measurements that provided only upper limits (37, 137–139).

Because of the low influx rate into the crust sample of only ~ 10 and ~ 70 ^{244}Pu atoms cm^{-2} Myr^{-1} on average (see **Figure 5a**, subpanel *ii*), only integrals over long time periods of several million years have been analyzed; i.e., the data were obtained from two thick layers that represent time periods of 4 to 5 Myr.

When compared with the total r-process content of heavy elements in the Galaxy, the Pu data suggest that regular core collapse SNe are not the dominant producers of heavy r-process nuclides for the past few hundred million years. Experimental data are consistent with a predominant contribution of compact-object mergers or a rare subset of SNe that are 100 to 1,000 times less frequent than core-collapse SNe. Nevertheless, the data would not exclude that more common SNe might contribute to some extent as a minor but frequent source to the total r-process budget in the Galaxy.

5.4. The $^{244}\text{Pu}/^{60}\text{Fe}$ Ratio

The combined search for ^{244}Pu and ^{60}Fe signals in the same archive links r-process nucleosynthesis and massive star (SN) nucleosynthesis. Despite the low temporal resolution in the ^{244}Pu

data obtained so far, the ^{244}Pu influx seems to correlate with the ^{60}Fe time profile. The data in **Figure 5a** give an atom ratio of $^{244}\text{Pu}/^{60}\text{Fe} = (3-5) \times 10^{-5}$.

We note the different half-lives of these two nuclides with ^{244}Pu being 30 times longer lived compared to ^{60}Fe . While ^{60}Fe decays within ~ 10 Myr to undetectable levels, ^{244}Pu could in principle be found in a few hundred-million-year-old archives. Also, considering ^{244}Pu 's slow decay, it could have been synthesized long before the ^{60}Fe -producing SNe. Swept up, it might have been moved toward the Solar System together with the ^{60}Fe , resulting in synchronous deposition.

Certainly, better time-resolved ^{244}Pu data are necessary to confirm or better understand the apparently concomitant influx of ^{60}Fe and ^{244}Pu .

5.5. Other Radioisotope Experiments

In 1996, Ellis et al. (60) suggested a number of other promising radionuclides that would provide additional information about the local ISM. This includes ^{53}Mn ($t_{1/2} = 3.7$ Myr), ^{26}Al (0.7 Myr), ^{182}Hf (8.9 Myr) and several more. While production yields in SNe would be similar to ^{60}Fe and much higher than for ^{244}Pu , detection of them was not successful or needs at least confirmation. Both ^{26}Al and ^{53}Mn measurements suffer so far from a prolific constant cosmogenic background production that might be much stronger than the interstellar influx, despite the fact that AMS of ^{26}Al and ^{53}Mn has improved significantly. In contrast to ^{60}Fe and ^{244}Pu , neither nuclide is rare on Earth.

5.5.1. Search for interstellar ^{53}Mn . The terrestrial production of ^{53}Mn is small but it is produced in larger quantities by cosmic ray interaction within the Solar System and is transported via (micro)meteorites to Earth at rather constant flux. Cosmogenic production is a factor of a few 100 higher compared to ^{60}Fe . That makes the detection of ^{53}Mn difficult as interstellar ^{53}Mn sits on top of this huge “naturally existing” ^{53}Mn signal. Interstellar ^{53}Mn is exclusively SN-produced.

The first evidence for interstellar ^{53}Mn was recently found for the same time period as that observed for the younger ^{60}Fe peak between 2 and 3 Myr before present (36). Data from four deep-sea crust samples were combined, and the measured data were found consistent with models for a mass range of 11–25 M_{\odot} for the SN progenitor (36, 141).

5.5.2. Search for interstellar ^{26}Al . ^{26}Al is another interstellar radionuclide candidate that is produced in massive stars and ejected into the ISM (30, 123, 142). It is, however, produced in large quantities naturally on Earth by cosmic-ray-induced nuclear reactions, and some deposition can also occur via interplanetary dust grains that also contain minor amounts of ^{26}Al .

Feige et al. (123) analyzed the same deep-sea sediment samples that showed a clear ^{60}Fe influx (23) for ages between 1.7 and 3.2 Myr, i.e., the younger larger ^{60}Fe peak. The data confirmed a dominant cosmogenic terrestrial component, and a lower limit for the atom ratio $^{60}\text{Fe}/^{26}\text{Al}$ of $0.18_{-0.08}^{+0.15}$ was deduced. This limit can be compared to the observed $^{60}\text{Fe}/^{26}\text{Al}$ γ -ray flux ratio in the ISM and with nucleosynthesis yields from models (30, 123).

5.5.3. Search for interstellar ^{129}I . ^{129}I is commonly studied with AMS, but modern levels are dominated by a global anthropogenic background from release of fission products in the environment. Detection of ^{129}I has been claimed in a FeMn crust (143) that is consistent with the background from fission of natural uranium in the ocean, with limits of $^{129}\text{I}/^{127}\text{I} \lesssim 10^{-11}$ in deep layers. This crust has not been independently dated but likely extends to 20 Myr ago or more and, so, likely overlaps with the ^{60}Fe and ^{244}Pu pulses.

RADIOACTIVITY DISTANCE

The formal similarity between the inverse square laws for radioisotope fluence and electromagnetic flux means that the “radioactivity distance” is the analog of the *luminosity distance* $D_L \sim \sqrt{L/F}$, with the radioisotope yield $M_{\text{ej},i}$ and fluence \mathcal{F}_i playing the roles of luminosity L and flux F , respectively.

6. CONSEQUENCES OF NEARBY SUPERNOVAE AND KILONOVAE

The detection of live, geologically recent extrasolar ^{60}Fe and ^{244}Pu offers a new probe of astrophysics and beyond. Here, we summarize the numerous implications.

6.1. Origin of ^{60}Fe and Distances to Supernovae

Equation 4 shows that radioisotope abundances (fluence as well as flux) depend on the distance to the source. We can therefore turn the problem around and use the observed ^{60}Fe fluence to estimate the distance to the explosion. If we neglect the distance dependence on the travel time from the source, the fluence simply varies as the inverse square of the distance, and so it is straightforward to solve for the “radioactivity distance” $D_{\text{rad}} \sim \sqrt{M_{\text{ej},60}/\mathcal{F}_{60}}$ (60, 144, 145) (see the sidebar titled Radioactivity Distance). We see that D_{rad} depends on the yield $M_{\text{ej},60}$, which is not measured empirically, and thus we must rely on the results from stellar models. In fact, this exercise allows us not only to systematically compare results for core-collapse SNe of different masses but also to survey the outcomes for all astrophysical sources of ^{60}Fe .

Figure 6 shows the radioactivity distance to the ^{60}Fe pulse 3 Myr ago, adapted from Reference 114. Results are plotted for a range of core-collapse SNe progenitor masses, but also for AGB stars, Type Ia SNe, and kilonovae. The adopted decay-corrected interstellar fluence is $\mathcal{F}_{60}^{\text{interstellar}} = 1.5 \times 10^8 \text{ cm}^{-2}$ as noted in Section 5.2, and a dust fraction $f = 3\%$ is assumed (146, 147). Horizontal lines show limits to the plausible distances: The lower limit at 10 pc is the SN “kill distance” inside of which a mass extinction would occur, and the upper limit around 160 pc is a typical fadeaway distance that is the maximum size of a SN remnant. We see that all core-collapse SNe and the electron capture SN fit comfortably between these limits. By contrast, Type Ia (thermonuclear) SNe and kilonovae fall inside of the kill distance, because they produce very little ^{60}Fe . These objects are thus ruled out. For AGB stars, the radioactivity distances are reasonable—AGB stars exist at these distances, but the transport of ^{60}Fe is an issue. These stars eject ^{60}Fe -bearing dust in winds with speeds an order of magnitude slower than a SN, and so it is not clear how the material can be delivered to Earth.

We conclude that core-collapse SNe are the only viable candidates and that a wide range of progenitor masses are possible given the uncertainties. The SN points also give a distance estimate of

$$D_{\text{rad}} \sim 12\text{--}150 \text{ pc.} \quad 7.$$

This range is large, but it is important to note that the calculation inputs—measured fluence and yields—have no astronomical distances built in. Thus, there was no guarantee that the radioactivity distance would fit in this plausible range at all. The agreement we find thus marks a nontrivial success: We have identified the astrophysical source of the ^{60}Fe as SN Plio and have a distance estimate. We also note that the earlier ^{60}Fe pulse, SN Mio, has a similar though somewhat smaller fluence, so the distance will be similar as well.

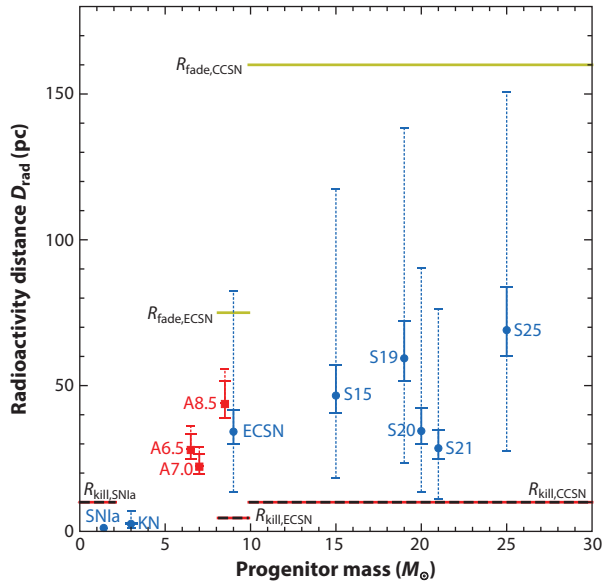


Figure 6

Radioactivity distance to SN Plio 3 Myr ago based on ^{60}Fe abundances (interstellar fluence) given in Section 5.2. Distances are shown for a range of progenitors. Solid and dotted error bars estimate uncertainty due to the ^{60}Fe fluence and also nuclear reaction rates, respectively. Also plotted are kill radius R_{kill} and the fadeaway radius R_{fade} that bound the SN distance from below and above, respectively. We see that core-collapse, ECSN, and AGB events lie between these limits, while a KN and SN Ia are ruled out. Abbreviations: An , AGB star of mass $n M_{\odot}$; ECSN, electron capture SN; KN, kilonova; SN, supernova; Sn , core-collapse SN of mass $n M_{\odot}$; SN Plio, Pliocene supernova; SNIa, Type Ia SNe. Figure adapted from Reference 114, with updated ^{60}Fe fluence and dust fraction $f = 3\%$.

Another possibility is that the SN enriches a cloud, through which the Sun later moves (23, 148, 149). This raises issues of cloud survival and ^{60}Fe transport to Earth (147), but in this picture, D_{rad} roughly corresponds to the distance from the SN to the cloud.

6.2. Implications for r-Process Nucleosynthesis

Because the actinides arise exclusively in the r-process, the detection of live ^{244}Pu is the smoking gun for a recent near-Earth r-process event (24). The observed ^{244}Pu flux overlaps with the two ^{60}Fe pulses, though the ^{244}Pu measurements have poor time resolution. The most straightforward interpretation would seem to be that the ^{244}Pu was made in the same SNe that produced ^{60}Fe . But as detailed in Section 3.1, SN models struggle to make the r-process, with particular difficulty making actinides. To study this scenario, Wang et al. (64) introduced two models in which SN actinide production occurs, either by modifications to standard neutrino physics or via the jets of magnetohydrodynamic explosions. Using the ^{244}Pu yields from these events, the resulting radioactivity distances around 100 pc overlaps with the results for ^{60}Fe .

Yet while the SN distance analysis is encouraging, it still requires an unusual SN, and the two ^{60}Fe pulses imply that this rarity happened twice in succession! It is conceivable that the two most recent nearby SNe both happened to be actinide producers, but such a coincidence invites consideration of other explanations.

An alternative is that the ^{244}Pu was made in a kilonova explosion, where actinide production is vigorous and its yields are large. Indeed the yields are so large that the naive radioactivity distance

required for a kilonova origin of the observed ^{244}Pu is $D_{\text{rad}} \gtrsim 10$ kpc, i.e., at least as far as the Galactic center. It is unlikely that radioisotopes can be transported over this distance. Instead, a possibility could be a two-step process, in which a kilonova explosion creates the ^{244}Pu and later SN explosions create the ^{60}Fe and help deliver both radioisotopes to Earth (24, 64). Reference 64 constructed a model in which the kilonova explosion enriches the Local Bubble that gave rise to the later SNe. This allows for the kilonova to occur at a $\sim 1\text{--}2$ kpc distance consistent with rate expectations.

Fortunately these two scenarios are testable, because the kilonova and SN r-process patterns are very different. As described in Section 3.1, SNe produce actinides weakly at best, so that ratios of lighter species to ^{244}Pu are much higher for SNe than for kilonovae. Thus, measurements of other r-process radioisotopes can discriminate between these scenarios. Indeed, ^{129}I data in a FeMn crust (143) already challenge the SN models in Equation 6, though this might also reflect the fragility of volatile iodine in dust grains. Future deep-sea and lunar (150) observations of this or other isotopes such as ^{182}Hf could offer powerful new insight into the site of the r-process.

6.3. Implications for Supernova Dust Production, Evolution, and Survival

We have seen in Section 3.3 that for SNe more distant than 10 pc, the blast does not reach the Earth and Moon. This is the case for SN Mio and Plio, with distances in Equation 7. Radioisotopes from these events therefore arrived in dust grains.

There is additional information about this process in the timescale for ^{60}Fe deposition. Sediment data place a lower limit on the ^{60}Fe flux duration of 1.65 Myr (23, 25, 136). This is a full order of magnitude longer than the timescale for the passage of a SN blast (109, 114). This implies that the dust grains moved independently from the gas in the SN remnant. This is consistent with the model of Fry et al. (151) in which SN dust grains can acquire electric charge and encounter a shocked, magnetized ISM.

Finally, we note another scenario proposed to account for the ^{60}Fe and ^{244}Pu detections: the possibility that the Solar System passed through a dense atomic cloud 2–3 Myr ago (149). If the cloud is very dense, it would compress the heliosphere to within the orbit of Mercury, exposing the Earth directly to the cloud material. ^{60}Fe and ^{244}Pu in the cloud would rain upon the Earth regardless of whether they are in the gas or dust phase. One can view this picture as a sort of modified two-step model, because it is still necessary that nearby SNe in the Local Bubble produce the radioisotopes and deliver them to the cloud. Observations of local cloud geometry, mass, and kinematics can shed light on this proposal.

6.4. Implications for the Solar Neighborhood: The Local Bubble

The detection of two distinct ^{60}Fe pulses implies that there were two recent SNe. This is consistent with a wealth of evidence that massive stars are “social”—they are often formed together in clusters, and furthermore many massive stars have a binary partner, often another massive star (152). Within the distance range given by Equation 7, two candidate star clusters have been suggested as the source of the ^{60}Fe . Scorpius–Centaurus (Sco-Cen) is the nearest OB association hosting a cluster of massive stars, and its distance 3 Myr ago was ~ 100 pc away (111). A smaller but closer cluster is the Tucana–Horologium Moving Group (153, 154). These occupy different regions of the sky, and so if the signal arrives as a plane wave, the distribution of ^{60}Fe on the Moon could distinguish them (113).

A nearby SN should create a black hole or neutron star, which likely receives a “kick” in the explosion. One can thus search for a nearby compact object moving at high speed across the sky

(high proper motion) (155). Indeed, the kinematics of the nearby radio pulsar PSR B1706-16 are consistent with an origin in Sco-Cen about 2 Myr ago (156). This is a candidate for SN Plio.

Fortunately, the Solar Neighborhood retains considerable information about the environment giving rise to nearby explosions—in particular, the Sun resides within the Local Bubble. That is, the Sun is presently near the center of a region $\gtrsim 100$ pc in size, filled with hot and low-density gas, and surrounded by a dense shell of cold gas and dust (157, 158). Models for the formation of the Local Bubble call for multiple SNe over the past ~ 10 Myr (159–161). For example, one of the Local Bubble simulations by the Berlin group (160) invokes 13 SNe over the past 13 Myr and includes calculations of the resulting ^{60}Fe flux. They find that each explosion leads to a distinct ^{60}Fe peak, supporting the conclusion that the two observed pulses point to two distinct explosions.

On scales greater than the Local Bubble, effects of inhomogeneity, mixing, and stochasticity continue to play important roles (162, 163). Our larger Galactic environment thus sets the context for the Local Bubble's formation and for possible enrichment by prior events that is modeled in the two-step scenario mentioned above.

6.5. Impact on the Heliosphere and Biosphere

Nearby SNe are among the most spectacular events the heliosphere can experience (164). As shown in **Figure 2**, the recent nearby SNe can leave the outer planets Uranus and Neptune directly exposed to the remnant. The SN should also create cosmic rays, bathing the heliosphere with newly accelerated high-energy particles.

These effects are unlikely to cause a mass extinction on Earth—the distance in Equation 7 is well beyond the ~ 10 -pc “kill radius” (Section 2)—but the stress to the biosphere may threaten the most vulnerable biota. While the visible light and ozone effects of the SN are small (47, 165), the cosmic-ray effects can be significant. The level of the cosmic-ray flux increase depends on the magnetic fields between Earth and the SN, which act to steer the charged particles. For plausible cases in which the fields in the Local Bubble are weak due to prior SN explosion, teraelectronvolt to petaelectronvolt cosmic rays can be enhanced by two orders of magnitude, leading to a muon flux increase by a factor of ~ 150 for many thousands of years (166). These have numerous effects (47), including a sharp rise in atmospheric ionization, increases in cancer and mutation rates, and possible climate forcing (21, 165).

Recent nearby SNe may also explain several anomalies in cosmic rays. An event ~ 2 Myr ago can account for the observed excess of positrons and antiprotons (167). This would also lead to observable features in the B/C ratio as a function of energy, which are testable (168).

7. PROSPECTS FOR FUTURE WORK

The study of near-Earth explosions is growing but still in its infancy, with many open questions and opportunities for future laboratory experiments, theoretical models, and astronomical observations.

- **Experiments:** New AMS measurements on extant and new radioisotopes can address a number of open questions. For isotopes already detected, perhaps the most pressing measurement is improved time resolution of ^{244}Pu to investigate the correlation with the ^{60}Fe pulses and to test the possibility of signals >10 Myr ago that would point to a prior explosion. Measurements of ^{244}Pu in sediments would allow for better $^{244}\text{Pu}/^{60}\text{Fe}$ ratios. Improved methods for finding astrophysical ^{26}Al and ^{53}Mn signals above the cosmogenic background would be welcome.

Artemis and *Chang'e* lunar sample returns can allow mapping of the ^{60}Fe distribution with latitude, particularly around the Lunar South Pole; this can probe the arrival directions of

the SN signal (113). Lunar measurements of ^{244}Pu and other r-process species benefit from a lack of anthropogenic contamination (150).

New radioisotopes offer new light on nucleosynthesis and dust astrophysics. Of particular interest are ^{129}I and ^{182}Hf , which can discriminate among possibilities for the origin of the r-process. In addition, ^{146}Sm can reach back to early mass extinctions and probe proton-rich SN nucleosynthesis.

Progress in isobar suppression may open up new options for the search for additional interstellar signatures. This includes new isobar-suppression capabilities in AMS (170–172). Other potential methods of interest are resonant-ionization mass spectrometry (RIMS) (118, 119) and atom trap trace analysis (ATTA) (120), which can provide ultrasensitivity.

Recent progress in AMS for the detection of ^{182}Hf seems promising (173–175). However, the present measurement background in AMS for other nuclides as identified by Ellis et al. (60), such as ^{107}Pd or some p-process nuclides (such as ^{92}Nb , ^{146}Sm) remains too high compared to the expected interstellar signature.

We note that high particle energies remain the most important factor in providing sufficient isobar suppression (121), which is the case for ^{60}Fe and ^{53}Mn , and becomes even more crucial for the medium-mass nuclides (e.g., ^{92}Nb , ^{107}Pd , ^{146}Sm).

A new large AMS system (14 to 20 MV with all the modern equipment and isobar suppression capabilities included) does not exist but would clearly represent a boost in both measurement efficiency and background reduction. It would bear an enormous potential for the detection of many nuclides not accessible today and would provide new opportunities for the search of ISM signatures in terrestrial and in lunar or Mars samples. Improved measurement sensitivities are also a crucial asset considering the planned sample return missions from the Moon as well as Mars.

The success in detecting recent nearby explosions impels searches at earlier times, possibly in association with mass extinctions. Nearby SNe have been suggested (176) as the cause for dramatic ozone reduction (177) during the Hangenberg Crisis extinction event 359 Myr ago at the end of the Devonian period. Possible radioisotope signals are ^{244}Pu (if made in SNe) and ^{146}Sm .

Nuclear physics experiments are crucial to improve radioisotope nucleosynthesis calculations. These include reaction rate measurements, such as $^{59}\text{Fe}(n, \gamma)^{60}\text{Fe}$, and also the Facility for Rare Isotope Beams (FRIB), which will measure rare isotopes relevant for the r-process (178).

- **Theoretical Models:** Increasingly realistic studies of stellar nucleosynthesis will remain crucial, particularly radioisotope production in SNe and kilonovae. A consensus among different models for SN ^{60}Fe production would be very useful, as would a firmer understanding of r-process radioisotope production, particularly actinides, in kilonovae and SNe. Improved models are needed for the formation and propagation of SN dust, and for transport of radioisotopes in the dynamic ISM. For kilonovae future work is needed to clarify radioisotope production, ejection, and propagation to Earth.
- **Astronomical Observations:** Infrared observations can help give a deeper understanding of SN dust and its evolution. We eagerly await JWST studies of dust in Galactic SN remnants, and of dust in high-redshift galaxies. These will inform improved theoretical models for dust production and propagation, including in magnetic fields.

At high energies, the upcoming MeV gamma-ray line mission, the Compton Spectrometer and Imager (COSI) (179), will probe ^{60}Fe and ^{26}Al nucleosynthesis across the Galaxy. On smaller scales, we look forward to improved maps of the Local Bubble in dust, gas, and stars. On the scale of the heliosphere, the proposed *Interstellar Probe* mission will blaze a new path

into the local ISM and provide a detailed picture of dust, gas, magnetic fields, and cosmic rays outside of the heliosphere.

Other messengers can shed important new light. Additional detections of kilonovae in concert with gravitational waves will provide invaluable information about their physics and nucleosynthesis. Similarly, cosmic-ray measurements of new radioisotopes including r-process species would open new windows.

8. CONCLUSIONS AND OUTLOOK

Deep-sea and lunar radioisotopes represent a new cosmic messenger and a new source of extrasolar material available for laboratory study. This opens a new window onto recent close-by cosmic explosions. There is a close and complementary relationship to presolar grains that also probe individual nucleosynthesis events (101) and early Solar System radioisotopes that sample nearby nucleosynthesis activity at the time of the Sun's birth (63).

There is a wealth of data on ^{60}Fe , which indicates multiple SNe exploded near the Earth. This picture is broadly consistent with our location in the Local Bubble, and has implications for many areas of astrophysics, as well as heliophysics, and possibly even biology.

The discovery of deep-sea ^{244}Pu indicates recent near-Earth r-process activity. This opens a new window on the physics of the r-process and its astrophysical site. Future ^{244}Pu measurements with better time resolution will be illuminating, particularly in concert with measurements of other radioisotopes.

It is therefore our view that this young field holds a bright future. The data in hand allow for a range of interpretations. We look forward to new insights and likely new surprises that will come with new laboratory measurements and astronomical observations as well as theoretical models—and perhaps above all—from new ideas.

DISCLOSURE STATEMENT

The authors are not aware of any affiliations, memberships, funding, or financial holdings that might be perceived as affecting the objectivity of this review.

ACKNOWLEDGMENTS

It is a pleasure to thank our collaborators and colleagues who made this work possible. The work of B.D.F. was supported by the National Science Foundation under grant AST-2108589. A.W. was supported by the Australian Research Council under grants DP180100495 and DP180100496.

LITERATURE CITED

1. Abbott BP, et al. *Phys. Rev. X* 9(3):031040 (2019)
2. Abbott R, et al. *Phys. Rev. X* 11(2):021053 (2021)
3. Aartsen MG, et al. (IceCube Collab.) *Science* 361(6398):eaat1378 (2018)
4. Abbasi R, et al. (IceCube Collab.) *Science* 378(6619):538 (2022)
5. Stein R, et al. *Nat. Astron.* 5:510 (2021)
6. Woosley SE, Heger A, Weaver TA. *Rev. Mod. Phys.* 74(4):1015 (2002)
7. Janka HT. *Annu. Rev. Nucl. Part. Sci.* 62:407 (2012)
8. Nomoto K, Kobayashi C, Tominaga N. *Annu. Rev. Astron. Astrophys.* 51:457 (2013)
9. Arcones A, Thielemann FK. *Astron. Astrophys. Rev.* 31:1 (2023)
10. Diehl R. In *Handbook of X-ray and Gamma-ray Astrophysics*, ed. C Bambi, A Santangelo. Singapore: Springer. https://link.springer.com/referenceworkentry/10.1007/978-981-16-4544-0_86-1#citeas (2022)
11. Wang W, et al. *Astrophys. J.* 889(2):169 (2020)

12. Metzger BD. *Living Rev. Relativity* 23:1 (2019)
13. Lattimer JM, Schramm DN. *Astrophys. J. Lett.* 192:L145 (1974)
14. Li LX, Paczyński B. *Astrophys. J. Lett.* 507:L59 (1998)
15. Abbott BP, et al. *Astrophys. J. Lett.* 848:L12 (2017)
16. Green DA, Gull SF. *Nature* 312(5994):527 (1984)
17. Luken KJ, et al. *Mon. Not. R. Astron. Soc.* 492(2):2606 (2020)
18. Murphey CT, Hogan JW, Fields BD, Narayan G. *Mon. Not. R. Astron. Soc.* 507:927 (2021)
19. Stephenson FR, Green DA. *Historical Supernovae and Their Remnants*. Oxford: Oxford Acad. (2002)
20. Knie K, et al. *Phys. Rev. Lett.* 83:18 (1999)
21. Knie K, et al. *Phys. Rev. Lett.* 93(17):171103 (2004)
22. Fitoussi C, et al. *Phys. Rev. Lett.* 101(12):121101 (2008)
23. Wallner A, et al. *Nature* 532(7597):69 (2016)
24. Wallner A, et al. *Science* 372(6543):742 (2021)
25. Ertel AF, Fry BJ, Fields BD, Ellis J. *Astrophys. J.* 947(2):58 (2023)
26. Koll D, et al. *Phys. Rev. Lett.* 123(7):072701 (2019)
27. Fimiani L, et al. *Phys. Rev. Lett.* 116(15):151104 (2016)
28. Binns WR, et al. *Science* 352(6286):677 (2016)
29. Fields B, et al. *Bull. Am. Astron. Soc.* 51(3):410 (2019)
30. Diehl R, et al. *Publ. Astron. Soc. Aust.* 38:e062 (2021)
31. Miller JA, et al. arXiv:2209.03497 (2022)
32. Korschinek G. In *Handbook of Supernovae*, ed. AW Alsabti, P Murdin, pp. 2419–30. Cham, Switz.: Springer (2017)
33. Wallner A. In *Handbook of Nuclear Physics*, ed. I Tanihata, H Toki, T Kajino. Singapore: Springer. https://doi.org/10.1007/978-981-15-8818-1_94-1 (2023)
34. Korschinek G, Faestermann T. *Eur. Phys. J. A* 59(3):52 (2023)
35. Koll D. *A 10-million year time profile of interstellar influx to Earth mapped through long-lived Fe-60 and Pu-244*. PhD Thesis, Aust. Nat. Univ./Tech. Univ. Dresden, Dresden, Ger. (2023)
36. Korschinek G, et al. *Phys. Rev. Lett.* 125(3):031101 (2020)
37. Wallner A, et al. *Nat. Comm.* 6:5956 (2015)
38. Schindewolf OH. *Der Zeitfaktor in Geologie und Paläontologie*. Stuttgart, Ger.: Schweizerbart Sci. Publ. (1950)
39. Schindewolf OH. *Neues Jahrbuch Geol. Paläontol. Monatshefte* 10:457 (1954)
40. Krassovskij VI, Šklovskij IS. *Nuovo Cim.* 8(S2):440 (1958)
41. Shklovsky IS. *Supernovae*. New York: Wiley-Intersci. (1968)
42. Ruderman MA. *Science* 184(4141):1079 (1974)
43. Reid GC, McAfee JR, Crutzen PJ. *Nature* 275:489 (1978)
44. Crutzen PJ, Bruhl C. *PNAS* 93(4):1582 (1996)
45. Gehrels N, et al. *Astrophys. J.* 585(2):1169 (2003)
46. Melott AL, Thomas BC. *Astrobiology* 11(4):343 (2011)
47. Thomas BC, et al. *Astrophys. J. Lett.* 826:L3 (2016)
48. Ellis J, Schramm DN. *PNAS* 92:235 (1995)
49. Brunton IR, et al. *Astrophys. J.* 947(2):42 (2023)
50. Atri D, Melott AL. *Radiat. Phys. Chem.* 80(6):701 (2011)
51. Atri D, Melott AL. *Astropart. Phys.* 53:186 (2014)
52. Melott AL, Marinho F, Paulucci L. *Astrobiology* 19(6):825 (2019)
53. Melott AL, Thomas BC. *J. Geol.* 127(4):475 (2019)
54. Kirkby J. *Surv. Geophys.* 28(5–6):333 (2007)
55. Melott A, Thomas BC, Fields BD. *Int. J. Astrobiol.* 19(5):349 (2020)
56. Russell D. *Nature* 229(5286):553 (1971)
57. Alvarez LW, Alvarez W, Asaro F, Michel HV. *Science* 208(4448):1095 (1980)
58. Konstantinov BP, Kocharov GE. *Sov. Phys. Dokl.* 10:1043 (1966)
59. Fields PR, et al. *Science* 167(3918):499 (1970)

60. Ellis J, Fields BD, Schramm DN. *Astrophys. J.* 470:1227 (1996)
61. Korschinek G, Faestermann T, Knie K, Schmidt C. *Radiocarbon* 38:68 (1996)
62. Adams SM, et al. *Astrophys. J.* 778(2):164 (2013)
63. Lugaro M, Ott U, Kereszturi Á. *Prog. Part. Nucl. Phys.* 102:1 (2018)
64. Wang X, et al. *Astrophys. J.* 923(2):219 (2021)
65. Diehl R, et al. *Nature* 439(7072):45 (2006)
66. Diehl R, et al. *Prog. Part. Nucl. Phys.* 127:103983 (2022)
67. Rugel G, et al. *Phys. Rev. Lett.* 103:072502 (2009)
68. Wallner A, et al. *Phys. Rev. Lett.* 114(4):041101 (2015)
69. Timmes FX, et al. *Astrophys. J.* 449:204 (1995)
70. Limongi M, Chieffi A. *Astrophys. J.* 647:483 (2006)
71. Tur C, Heger A, Austin SM. *Astrophys. J.* 718:357 (2010)
72. Limongi M, Chieffi A. *Astrophys. J. Suppl.* 237:13 (2018)
73. Sukhbold T, et al. *Astrophys. J.* 821:38 (2016)
74. Curtis S, et al. *Astrophys. J.* 870:2 (2019)
75. Jones SW, et al. *Mon. Not. R. Astron. Soc.* 485(3):4287 (2019)
76. Lawson TV, et al. *Mon. Not. R. Astron. Soc.* 511:886 (2022)
77. Lugaro M, Karakas AI. *New Astron. Rev.* 52(7–10):416 (2008)
78. Doherty CL, et al. *Mon. Not. R. Astron. Soc.* 437:195 (2014)
79. Wanajo S, Janka HT, Müller B. *Astrophys. J. Lett.* 774:L6 (2013)
80. Nomoto K, Thielemann FK, Yokoi K. *Astrophys. J.* 286:644 (1984)
81. Woosley SE. *Astrophys. J.* 476(2):801 (1997)
82. Burbidge EM, Burbidge GR, Fowler WA, Hoyle F. *Rev. Mod. Phys.* 29(4):547 (1957)
83. Cameron AGW. *Publ Astron. Soc. Pac.* 69(408):201 (1957)
84. Thielemann FK, Eichler M, Panov I, Wehmeyer B. *Annu. Rev. Nucl. Part. Sci.* 67:253 (2017)
85. Frebel A. *Annu. Rev. Nucl. Part. Sci.* 68:237 (2018)
86. Cowan JJ, et al. *Rev. Mod. Phys.* 93:015002 (2021)
87. Banerjee P, Qian YZ, Heger A. *Astrophys. J.* 865(2):120 (2018)
88. Ji AP, Frebel A. *Astrophys. J.* 856(2):138 (2018)
89. Kobayashi C, Karakas AI, Lugaro M. *Astrophys. J.* 900(2):179 (2020)
90. Shibata M, Hotokezaka K. *Annu. Rev. Nucl. Part. Sci.* 69:41 (2019)
91. Cowperthwaite PS, et al. *Astrophys. J. Lett.* 848(2):L17 (2017)
92. Côté B, et al. *Astrophys. J.* 875(2):106 (2019)
93. Pruet J, Woosley SE, Hoffman RD. *Astrophys. J.* 586(2):1254 (2003)
94. Surman R, McLaughlin GC, Hix WR. *Astrophys. J.* 643(2):1057 (2006)
95. Winteler C, et al. *Astrophys. J. Lett.* 750:L22 (2012)
96. Mösta P, et al. *Astrophys. J.* 864(2):171 (2018)
97. Siegel DM, Barnes J, Metzger BD. *Nature* 569(7755):241 (2019)
98. Reichert M, et al. *Mon. Not. R. Astron. Soc.* 501(4):5733 (2021)
99. Draine BT. *Physics of the Interstellar and Intergalactic Medium*. Princeton, NJ: Princeton Univ. Press (2011)
100. Matsuura M, et al. *Science* 333(6047):1258 (2011)
101. Clayton DD, Nittler LR. *Annu. Rev. Astron. Astrophys.* 42:39 (2004)
102. Bianchi S, Schneider R. *Mon. Not. R. Astron. Soc.* 378(3):973 (2007)
103. Ackermann M, et al. *Science* 339(6121):807 (2013)
104. Malkov MA, Drury LO. *Rep. Prog. Phys.* 64(4):429 (2001)
105. Ellison DC, Drury LO, Meyer JP. *Astrophys. J.* 487:197 (1997)
106. Montes G, et al. *Astrophys. J.* 830:12 (2016)
107. Takami H, Nozawa T, Ioka K. *Astrophys. J. Lett.* 789:L6 (2014)
108. Gall C, et al. *Astrophys. J. Lett.* 849(2):L19 (2017)
109. Miller JA, Fields BD. *Astrophys. J.* 934:32 (2022)
110. Fields BD, Athanassiadou T, Johnson SR. *Astrophys. J.* 678:549 (2008)
111. Benitez N, Maiz-Apellániz J, Canelles M. *Phys. Rev. Lett.* 88(8):081101 (2002)

112. Athanassiadou T, Fields BD. *New Astron.* 16(4):229 (2011)
113. Fry BJ, Fields BD, Ellis JR. *Astrophys. J.* 827:48 (2016)
114. Fry BJ, Fields BD, Ellis JR. *Astrophys. J.* 800:71 (2015)
115. Kutschera W. *Int. J. Mass Spectrom.* 349–350:203 (2013)
116. Synal HA. *Int. J. Mass Spectrom.* 349–350:192 (2013)
117. Kutschera W, Jull A, Paul M, Wallner A. *Rev. Mod. Phys.* In press (2023)
118. Wendt KD. *Eur. J. Mass Spectrom.* 8(4):273 (2002)
119. Trappitsch R, et al. *50th Lunar Planet. Sci. Conf. 2019 (LPI Contrib. No. 2132)* (2019)
120. Lu Z. A primer on atom trap trace analysis (ATTA). *Laser Laboratory for Trace Analysis and Precision Measurements*. <https://atta.ustc.edu.cn/en-us/events/attaprimer.html> (2022)
121. Wallner A, et al. *Nucl. Instrum. Methods Phys. Res. B* 534:48 (2023)
122. Koll D, et al. *Nucl. Instrum. Methods Phys. Res. Sect. B* 438:180 (2019)
123. Feige J, et al. *Phys. Rev. Lett.* 121(22):221103 (2018)
124. Vockenhuber C, et al. *Nucl. Instrum. Methods Phys. Res. Sect. B* 294:382 (2013)
125. Hotchkis MAC, et al. *Nucl. Instrum. Methods Phys. Res. B* 438:70 (2019)
126. Cole AL, et al. *Astrophys. J.* 652(2):1763 (2006)
127. Hein J, Koschinsky A. In *Treatise on Geochemistry*, ed. HD Holland, KK Turekian, pp. 273–91. Oxford: Elsevier. 2nd ed. (2014)
128. Segl M, et al. *Nature* 309(5968):540 (1984)
129. Basu S, Stuart FM, Schnabel C, Klemm V. *Phys. Rev. Lett.* 98(14):141103 (2007)
130. Stuart FM, Lee MR. *Chem. Geol.* 322–323:209 (2012)
131. Koll Dominik, et al. *EPJ Web Conf.* 260:11022 (2022)
132. Graham DW, Konrad K. *Geochim. Cosmochim. Acta* 336:177 (2022)
133. Korschinek G, et al. *Nucl. Instrum. Methods Phys. Res. Sect. B* 268(2):187 (2010)
134. Korschinek G, Faestermann T. *Nucl. Instrum. Methods Phys. Res. Sect. B* 438:148 (2019)
135. Wallner A, et al. *PNAS* 117(36):21873 (2020)
136. Ludwig P, et al. *PNAS* 113(33):9232 (2016)
137. Paul M, et al. *Astrophys. J.* 558:L133 (2001)
138. Paul M, et al. *J. Radioanal. Nucl. Chem.* 272:243 (2007)
139. Wallner C, et al. *Nucl. Instrum. Methods Phys. Res. Sect. B* 172:333 (2000)
140. Wallner C, et al. *New Astron. Rev.* 48(1–4):145 (2004)
141. Woosley SE, Weaver TA. *Astrophys. J. Suppl.* 101:181 (1995)
142. Diehl R, et al. *Astron. Astrophys.* 611:A12 (2018)
143. Ji L, et al. *Acta Oceanol. Sin.* 34(20150802):13 (2015)
144. Fields BD, Ellis J. *New Astron.* 4(6):419 (1999)
145. Fields BD, Hochmuth KA, Ellis J. *Astrophys. J.* 621(2):902 (2005)
146. Marassi S, et al. *Mon. Not. R. Astron. Soc.* 484(2):2587 (2019)
147. Slavin J. *J. Phys.: Conf. Ser.* 1620:012019 (2020)
148. Chaikin E, Kaurov AA, Fields BD, Correa CA. *Mon. Not. R. Astron. Soc.* 512:712 (2022)
149. Opher M, Loeb A. arXiv:2202.01813 (2022)
150. Wang X, et al. *Astrophys. J.* 948:113 (2023)
151. Fry BJ, Fields BD, Ellis JR. *Astrophys. J.* 894(2):109 (2020)
152. Zinnecker H, Yorke HW. *Annu. Rev. Astron. Astrophys.* 45:481 (2007)
153. Mamajek EE. In *Triggered Star Formation in a Turbulent ISM*, Vol. 237, ed. BG Elmegreen, J Palous, p. 442. Cambridge, UK: Cambridge Univ. Press (2007)
154. Hyde M, Pecaut MJ. *Astron. Nachr.* 339:78 (2018)
155. Tetzlaff N, Neuhäuser R, Hohle MM, Maciejewski G. *Mon. Not. R. Astron. Soc.* 402(4):2369 (2010)
156. Neuhäuser R, Gießler F, Hambaryan VV. *Mon. Not. R. Astron. Soc.* 498:899 (2020)
157. Frisch PC, Redfield S, Slavin JD. *Annu. Rev. Astron. Astrophys.* 49:237 (2011)
158. Zucker C, et al. *Nature* 601(7893):334 (2022)
159. Smith RK, Cox DP. *Astrophys. J. Suppl.* 134(2):283 (2001)
160. Breitschwerdt D, et al. *Nature* 532(7597):73 (2016)

161. Schulreich M, Breitschwerdt D, Feige J, Dettbarn C. *Galaxies* 6:26 (2018)
162. Hotokezaka K, Piran T, Paul M. *Nat. Phys.* 11(12):1042 (2015)
163. Wehmeyer B, et al. *Astrophys. J.* 944(2):121 (2023)
164. Müller HR, Frisch PC, Florinski V, Zank GP. *Astrophys. J.* 647(2):1491 (2006)
165. Orgeira MJ, Herrera VMV, Cappellotto L, Compagnucci RH. *Int. J. Earth Sci.* 111(4):1357 (2022)
166. Melott AL, et al. *Astrophys. J.* 840(2):105 (2017)
167. Kachelrieß M, Neronov A, Semikoz DV. *Phys. Rev. Lett.* 115(18):181103 (2015)
168. Kachelrieß M, Neronov A, Semikoz DV. *Phys. Rev. D* 97(6):063011 (2018)
169. Deleted in proof
170. Liu Y, Beene JR, Havener CC, Liang JF. *Appl. Phys. Lett.* 87(11):113504 (2005)
171. Lachner J, et al. *Int. J. Mass Spectrom.* 465:116576 (2021)
172. Martschini M, et al. *Radiocarbon* 64(3):555 (2022)
173. Vockenhuber C, et al. *New Astron. Rev.* 48(1–4):161 (2004)
174. Forstner O, et al. *Nucl. Instrum. Methods Phys. Res. Sect. B* 269(24):3180 (2011)
175. Martschini M, et al. *EPJ Web Conf.* 232:02003 (2020)
176. Fields BD, et al. *PNAS* 117(35):21008 (2020)
177. Marshall JE, Lakin J, Troth I, Wallace-Johnson SM. *Sci. Adv.* 6(22):eaba0768 (2020)
178. Horowitz CJ, et al. *J. Phys. G Nucl. Phys.* 46(8):083001 (2019)
179. Tomsick J. (COSI Collab.) *Proc. Sci. ICRC2021*:652 (2022)